



|                                  |  |
|----------------------------------|--|
| <b>Publication Year</b>          | 2016   |
| <b>Acceptance in OA</b>          | 2020-05-05T15:30:42Z   |
| <b>Title</b>                     | Field Measurements of Terrestrial and Martian Dust Devils  |
| <b>Authors</b>                   | Murphy, Jim, Steakley, Kathryn, Balme, Matt, Deprez, Gregoire, ESPOSITO, Francesca, Kahanpää, Henrik, Lemmon, Mark, Lorenz, Ralph, Murdoch, Naomi, Neakrase, Lynn, Patel, Manish, Whelley, Patrick |
| <b>Publisher's version (DOI)</b> | 10.1007/s11214-016-0283-y  |
| <b>Handle</b>                    | <a href="http://hdl.handle.net/20.500.12386/24523">http://hdl.handle.net/20.500.12386/24523</a>  |
| <b>Journal</b>                   | SPACE SCIENCE REVIEWS  |
| <b>Volume</b>                    | 203  |

# Field Measurements of Terrestrial and Martian Dust Devils

Jim Murphy<sup>1</sup> · Kathryn Steakley<sup>1</sup> · Matt Balme<sup>2</sup> · Gregoire Deprez<sup>3</sup> ·  
Francesca Esposito<sup>4</sup> · Henrik Kahanpää<sup>5,6</sup> · Mark Lemmon<sup>7</sup> · Ralph Lorenz<sup>8</sup> ·  
Naomi Murdoch<sup>9</sup> · Lynn Neakrase<sup>1</sup> · Manish Patel<sup>2</sup> · Patrick Whelley<sup>10</sup>

Received: 10 May 2016 / Accepted: 24 August 2016  
© Springer Science+Business Media Dordrecht

**Abstract** Surface-based measurements of terrestrial and martian dust devils/convective vortices provided from mobile and stationary platforms are discussed. Imaging of terrestrial dust devils has quantified their rotational and vertical wind speeds, translation speeds, dimensions, dust load, and frequency of occurrence. Imaging of martian dust devils has provided translation speeds and constraints on dimension, but only limited vertical constraints on vertical motion within a vortex. The longer mission durations on Mars afforded by long operating robotic landers and rovers have provided statistical quantification of vortex occurrence (time-of-sol, and recently seasonal) that has until recently not been a primary outcome of more temporally limited terrestrial dust devil measurement campaigns. Terrestrial measurement campaigns have included a more extensive range of measured vortex parameters (pressure, wind, morphology, etc.) than have martian opportunities, with electric field and direct measure of abundance not yet obtained on Mars. No martian robotic mission has yet provided contemporaneous high frequency wind and pressure measurements. Comparison of measured terrestrial and martian dust devil characteristics suggests that martian dust devils are larger and possess faster maximum rotational wind speeds, that the absolute magnitude of the pressure deficit within a terrestrial dust devil is an order of magnitude greater

✉ J. Murphy  
[murphy@nmsu.edu](mailto:murphy@nmsu.edu)

<sup>1</sup> New Mexico State University, Las Cruces, NM, USA

<sup>2</sup> Open University, Milton Keynes, UK

<sup>3</sup> Laboratoire Atmosphères, Guyancourt, France

<sup>4</sup> INAF, Osservatorio Astronomico di Capodimonte, Naples, Italy

<sup>5</sup> Finnish Meteorological Institute, Helsinki, Finland

<sup>6</sup> Aalto University/School of Electrical Engineering, Espoo, Finland

<sup>7</sup> Texas A&M University, College Station, TX, USA

<sup>8</sup> Johns Hopkins University Applied Physics Lab, Laurel, MD, USA

<sup>9</sup> ISAE-SUPAERO, Toulouse University, Toulouse, France

<sup>10</sup> NASA Goddard Space Flight Center, Greenbelt, MD, USA

51 than a martian dust devil, and that the time-of-day variation in vortex frequency is similar.  
52 Recent terrestrial investigations have demonstrated the presence of diagnostic dust devil sig-  
53 nals within seismic and infrasound measurements; an upcoming Mars robotic mission will  
54 obtain similar measurement types.

55  
56 **Keywords** Dust devils

## 57 58 59 60 **1 Introduction**

61  
62 Dust devils are small diameter, surface bordering, vertically aligned atmospheric convective  
63 vortices made visible by their entrainment of dust lifted from the surface (Fig. 1). Historic  
64 anecdotal reports (Lorenz et al. 2016) indicate qualitative awareness of these phenomena  
65 extending for millennia into the past. Quantitative awareness is more recent (Ives 1947;  
66 Wyatt 1954). Dust devils are one mechanism that emplaces dust into atmospheric suspen-  
67 sion, affecting air quality, atmospheric clarity, possible hazardous conditions to low flying  
68 aircraft, etc. Dust devils have also been identified on Mars, where they play a possibly sub-  
69 stantial role in maintaining that planet's persistent atmospheric dust load, especially during  
70 the orbital aphelion season (Kahre et al. 2006). It is only during the modern era of scientific  
71 investigation and measurement that the true physical understanding of these phenomena  
72 on both planets have been achieved. In this presentation we focus upon the quantitative  
73 characterization of dust devils, on both Earth and Mars, which have resulted in our current  
74 understanding of their physical attributes.

75  
76 Terrestrial dust devil attributes measured to date include winds (radial, azimuthal, verti-  
77 cal), translation speed, shape/height/width (visualized by suspended dust), central pressure  
78 deficit, dust load and its radial and vertical structure and particle size distribution, electric  
79 field, and surface dust lifting rate. Measurements have been provided in situ from mobile  
80 and stationary instrumented platforms (either individually or in a network) and/or remotely  
81 imaged at visible wavelengths, with some infrared wavelength measurements also available.  
82 Measurements obtained from Mars' surface include both in situ (pressure, wind) and re-  
83 motely imaged (visible imaging) characterization, but remain deficient in other areas (elec-  
84 tric field, dust lifting rate). While terrestrial field campaigns have usually been, until recently,  
85 of short time extent (days, weeks), martian 'campaigns' (robotic exploration missions) have  
86 been more time extended, limited by the lifetime of the mission or its most applicable in-  
87 struments. However, no martian mission has provided continuous sampling for all forms  
88 of observations, though the Mars Phoenix Lander did provide almost continuous 0.5 Hz  
89 sampling of its meteorology measurements.

90  
91 Balme and Greeley (2006) provided an extensive dust devil review. Here we emphasize  
92 subsequent gained knowledge in addition to reiterating their primary foci.

93  
94 In Sect. 2 below we describe primarily surface based imaging characterization of ter-  
95 restrial dust devils (Sect. 2.1) from a variety of field campaigns, followed by surface based  
96 imaging characterization of martian dust devils (Sect. 2.2) provided by the seven spacecraft  
97 that have operated/are operating there. [Note that Fenton et al. (2016) in this collection of  
98 papers addresses dust devil remote sensing from non-surface based measurements such as  
99 those provided by orbiting spacecraft.] This is followed in Sect. 3 by presentation of in  
100 situ measurements of terrestrial dust devils (Sect. 3.1) and martian dust devils (Sect. 3.2).

**Fig. 1** Image of a terrestrial dust devil in Eldorado Valley, Nevada, USA, 2009. Notice, for scale, the ‘chase vehicle’ positioned at the lower left of the dust devil. Image provided by M. Balme



Emphasis is placed upon the types of measurements obtained and their indication of mean characteristics and identified extrema. [Assessment of dust devil population statistics is provided in the accompanying paper by Lorenz and Jackson (2016).] The terrestrial measurements span a large quantity of literature covering a large number of measurements opportunities. The martian literature is more limited and the measurement opportunities much more discrete than their terrestrial counterparts. The martian instrumentation is discussed in some detail. In Sect. 4 we provide a brief discussion of terrestrial versus martian dust devils. In Sect. 5 we address the topic of future measurements desired for a more complete characterization of terrestrial and martian dust devils. Concluding remarks are presented in Sect. 6.

## 2 Surface Obtained Imaging of Dust Devils

Most studies of dust devils on Earth have used either (i) an in-situ sampling methodology (i.e. by ‘chasing’ a dust devil with an instrumented vehicle, or by waiting for a dust devil to approach one or more immobile instrument stations), or (ii) a local remote sensing methodology, in which one or more observers document the local time, size, dust load, morphology, etc. of dust devils as they occur within some kind of fixed study area. Some studies have used a combination of these approaches by deploying both observers and in-situ instruments.

The main challenge for any field study is that dust devils are inherently changeable and somewhat unpredictable. Hence, measurements of size, lifetime and dustiness of a given dust devil are difficult to make—some dust devils start small and grow larger and dustier and persist for many minutes, whereas similar starting examples can disappear without a trace after just a few seconds. This presents a challenge for any qualitative study as “summarising” any dust devil with a few simple parameters is sometimes impossible. Another problem is that dust devils can travel quickly, and can move into and out of a defined study area (or even the entire field of view of an observer) during their lifetime. Similarly, studies

**Table 1** Terrestrial dust devil observed characteristics

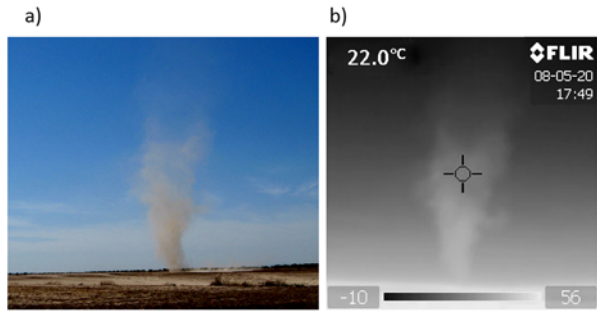
| Parameter                                       | Best observations or measurements   | Key literature  |
|---|---|---|
| Size (diameter)                                 | 1 to > 100 m; Strongly skewed size frequency distribution: small dust devils much more common than large; examples > 300 m are very uncommon  | Carroll and Ryan (1970); Sinclair (1965); Lorenz (2011)                         |
| Size (height)                                   | 5 m to > 1000 m; only about 10 % are > 300 m  | Sinclair (1965); Bell (1967); Flower (1936)                                     |
| Lifetime  | Seconds to minutes; larger dust devils have longer lifetimes; some reports of large dust devils lasting several hours   | Flower (1936); Snow and McClelland (1990); Pathare et al. (2010); Lorenz (2013) |
| Morphology                                      | Columnar, disordered or v-shaped; columnar vortices often include a v-shaped 'sand skirt'; larger dust devils often include sub-vortices  | Metzger (1999)  |
| Rotation sense                                  | Equally clockwise and counter-clockwise   | Flower (1936); Carroll and Ryan (1970)  |
| Wind speeds (peak horizontal) at 2 m height     | Usually peak at 5–10 $\text{m s}^{-1}$ ; recorded peak winds of up to 25 $\text{m s}^{-1}$ are not unusual  | Ryan and Carroll (1970); Balme et al. (2003)                                    |
| Wind speeds (peak vertical) at 1.0–4.5 m height | Usually ~ 25 % of peak horizontal winds; most peak measurements < 5 $\text{m s}^{-1}$ ; rare values of ~ 15 $\text{m s}^{-1}$ measured  | Sinclair (1973); Fitzjarrald (1973); Metzger (1999); Metzger et al. (2011)      |
| Horizontal translation speed                    | 10–20 % greater than ambient wind speeds measured at 10 m height; values of 0 – –10 $\text{m s}^{-1}$ common; rare observations of values > 20 $\text{m s}^{-1}$  | Balme et al. (2012)   |
| Dust loading at 2 m height                      | Mean values (i.e., averaged across a profile within each dust devil rather than peak measurement) of 0.8–42 $\text{mg m}^{-3}$ measured for fine particles (0–10 mm diameter); mean values of up to 6–875 $\text{mg m}^{-3}$ for total suspended load; average values across > 20 dust devils reveal particle load of ~ 44 $\text{mg m}^{-3}$ for fine particles, ~ 300 $\text{mg m}^{-3}$ for total suspended load | Metzger et al. (2011)   |
| Core temperature excursion                      | Wide range of temperature excursions measured—probably due to variations in sensor type; excursions of 1–5 °C common; larger excursions of > 20 °C reported   | Metzger (1999); Tratt et al. (2003); Sinclair (1964); Sinclair (1973)           |
| Core pressure excursion (DP)                    | Mobile sampling systems appear to give larger values: ~ 1–10 mbar; fixed monitoring stations give values < 1.5 mbar   | Sinclair (1973); Metzger (1999); Lorenz and Lanagan (2014)                      |
| Electric fields                                 | Field of ~ 10–100 kV/m measured; early measurements hampered by field reaching measurement limit of instrument  | Jackson and Farrell (2006); Renno et al. (2004); Esposito et al. (2016a, 2016b) |

relying on untended instruments can find it hard to distinguish between a population of long-lived dust devils and a population of more frequently occurring, but short lived dust devils.

A summary of observed characteristics is provided in Table 1.

AUTHOR'S PROOF

**Fig. 2** (a) A digital camera image of a dust devil in Eloy, AZ in summer 2008. (b) A thermal image of the same devil a few seconds later with a FLIR Infracam hand-held thermal imager (240 × 240 pixels). Note that the image scale is not the same as in the optical image. The bar at the base of the thermal image indicates the brightness temperature grey scale in Celsius



## 2.1 Remotely Observed Terrestrial Dust Devil Characteristics

### 2.1.1 Morphology

Dust devil morphology has been measured almost exclusively by surface based remote imaging observation (Figs. 1 and 2). As described by Lorenz et al. (2016), dust devils have been observed for many centuries and many authors describe them as “dusty-columns” or “upright whirlwinds”. However, as shown by Metzger (1999), many dust devils do not have this ‘classic’ form; many are simply disordered clouds of barely-spinning dust, others are more-rapidly spinning, v-shaped cones of entrained dust and sand, and others do have the well-known, rapidly-spinning columnar shape. In a study in Nevada, USA, Metzger (1999) found that only about 4 % of observed dust devils have a columnar shape. Even for those with columnar vortices, their morphology can differ: some have a clear core, others do not; some include a v-shaped “skirt” at their base, but others do not. Finally, some dust devils include sub-vortices that have their own centre of rotation but orbit the main circulation or which trail in their wake (e.g., Williams 1948; Ryan and Carroll 1970; Hallett and Hoffer 1971; Sinclair 1973; Metzger 1999). In many cases, the main circulation is barely dust-charged at all, so in these cases it is difficult to judge whether this is one large dust devil with subsidiary rotational elements, or a group of interacting smaller dust devils.

Most dust devils are higher than their widths. Hess and Spillane (1990) suggest that most are at least five times higher than their width, but again, many opposing observations exist. For those dust devils tall enough that a vertical structure can be observed, Sinclair (1966) provides a still-relevant summary: Region 1 is the zone nearest the ground, is heavily particle-loaded and often has a v-shaped form (Metzger 1999, refers to this as a “sand-skirt”). Region 2, at intermediate height, is the near- vertical column of rotating dust. Region 3, aloft, is where the rotation decays and where the dust devils “fades” into the ambient atmosphere. These regions have been associated with different flow regimes (see, for example, Balme and Greeley 2006, Fig. 9): region 1 is where the majority of the radial inflow occurs, while Region 2 is characterised by rotation and uplift, and Region 3 has poorly characterised flows as here the structure dissipates.

### 2.1.2 Size

Dust devils on Earth range in size from a few metres in diameter and height to 100 s of metres in diameter and perhaps more than a kilometre in height. While estimates or measurements of diameter are relatively easy to obtain, determining dust devil height is more difficult, especially from surface observations. Also, it must be recognised that dust devil height refers

251 to the observable dust column height, as opposed to the height of any circulation associ-  
252 ated with the dust devil. For the visible column, estimates suggest that most dust devils  
253 are less than 50 m high, with only about 8 % extending higher than 300 m (Sinclair 1965;  
254 Flower 1936; Williams 1948). However, observations made from the air identify taller dust  
255 devils that are 1–2.5 km in height (Bell 1967). Finally, Sinclair (1966) notes that measurable  
256 vertical wind speed and temperature excursions occur above large dust devils at heights of  
257 2–4 km. However, it is not clear that these represent the upper parts of a dust devil per-se,  
258 or instead are associated with a broader circulation in which the dust devil is embedded.

259 The diameter-frequency of dust devils has been the subject of much study, with method-  
260 ologies including simple “by-eye” observer surveys to more sophisticated studies that use  
261 time-lapse cameras or arrays of meteorology data. As noted by Lorenz (2011), most visual  
262 surveys (e.g., Sinclair 1965, 1969; Ryan and Carroll 1970; Snow and McClelland 1990) re-  
263 port that small dust devils are underreported by observers. Possible exceptions to this are  
264 the studies of Carroll and Ryan (1970), Pathare et al. (2010) and Balme et al. (2012), which  
265 both used small (1 km by 1 km or smaller) study areas. Several recent studies have focused  
266 on power law and other functional forms that best describe the dust devil size-frequency  
267 population (e.g., Kurgansky 2006; Lorenz 2009, 2011; Pathare et al. 2010)—a topic which  
268 is described in more detail by Lorenz and Jackson (2016) in this issue.

269 What is clear from all these studies is that the diameter-frequency distribution of dust  
270 devils is significantly skewed, with far more small dust devils occurring than large. Hence,  
271 the concept of an “average” dust devil diameter is not necessarily a useful one. What is clear,  
272 though, is that dust devils narrower than 5–6 meters in diameter are far more common than  
273 those wider than 10–12 m, and that dust devils wider than 50 m are actually rather rare (e.g.  
274 Balme and Greeley 2006, Fig. 3; Lorenz 2011, Table 1).

### 275 *2.1.3 Translation Speeds*

276 Compared with Mars, few measurements of translational speed of terrestrial dust devils have  
277 been made. This is mainly due to the lack of top-down remote sensing of dust devils available  
278 for the Earth. Some ad-hoc measurements were made in the twentieth century (e.g. Crozier  
279 1970) but the only focussed study, aimed solely at measuring the forward motion of dust  
280 devils, is that of Balme et al. (2012), who used stereo photography of dust devils to locate  
281 them in time and space. Multiple observations were made of each dust devil, thus allowing  
282 a path and thus a velocity to be calculated for each dust devil. In addition, as Balme et al.  
283 (2012) employed two 10 m high meteorology masts within their study area, they were able  
284 to correlate dust devil motion with ambient wind speed and direction. During the 10 days  
285 of field sampling, covering two calendar years and two study sites, translation speeds of  
286 between 1 and 15 ms<sup>-1</sup> were measured for more than 100 dust devils.

287 Balme et al. (2012) found that dust devils translated in the same direction as ambient  
288 wind, and that the dust devil forward speed correlated well with ambient wind speed. In  
289 fact, they found that dust devils travel at about the same speed as the boundary layer winds a  
290 few tens of metres above ground. Interestingly, no correlation of translation speed with dust  
291 devil diameter was found. Therefore, Balme et al. (2012) conclude that dust devil forward  
292 motion is a good proxy for the wind field, and that dust devil motions is governed almost  
293 solely by local wind patterns—a finding that could prove to be important for Mars, where  
294 few meteorology data are available.

### 295 *2.1.4 Rotational and Vertical Speeds Within Dust Devils*

296 Measurement of the swirling winds within dust devils has generally been accomplished  
297 using in-situ sampling, though particle imaging velocimetry (Ito and Niino 2014) and re-  
298  
299  
300

301 mote measurements using Light Detection And Ranging, or “LIDAR” (e.g., Schwiesow  
302 et al. 1977; Bluestein and Pazmany 2000) have also been employed. Obtaining statistically  
303 significant quantities of data is challenging for two main reasons. Firstly, even the most ef-  
304 ficient sampling methodology (arguably, the mobile sampling platform approach) will only  
305 be able to sample a few dust devils per day, due to the short-lived and random nature of the  
306 phenomenon. Fixed sampling positions mean an even lower number of samples are likely,  
307 although this problem can be ameliorated by using many sensors in large arrays, or by sam-  
308 pling for very long periods of time. It is possible that dedicated LIDAR studies could also  
309 gather large quantities of data but to date no such attempts have been made. To date, the  
310 largest published study is that of Ryan and Carroll (1970), who sampled 80 dust devils. An-  
311 other more recent large dataset exists (see preliminary report in Metzger et al. 2011) and  
312 includes more than 50 measurements from mobile in-situ sampling. However, these data  
313 are yet to be formally published. Aside from these two examples, individual studies usually  
314 report fewer than twenty encounters (Balme and Greeley 2006).

315 Both in-situ and remote sampling of wind speeds share the second problem—smaller  
316 and/or shorter-lived dust devils are harder to sample, and therefore are likely to be under  
317 represented in the data. This problem is likely to affect mobile “chase” strategies most sig-  
318 nificantly, as only the larger and longer-lived dust devils can be caught and penetrated to  
319 acquire data. Similarly, fixed-position remote-sensing studies are liable to target the most  
320 easily seen dust devils and could easily miss small, less dusty examples. The remaining  
321 methodology—that of fixed long-term meteorology stations—should be able to remove this  
322 sample bias, but again there is the issue of detectability, although this time the problem  
323 is how to tease out “detections” from the data. Significant progress has been made in this  
324 area recently; by using a single meteorology station and a theoretical dust devil ‘signature’,  
325 Lorenz (2016) was able to reconstruct peak wind speeds (and other signature parameters)  
326 and miss distance (i.e. the distance from the dust devil core to the sensor) for 27 dust devil  
327 events in 16 days of field time. However, the calculated diameters for these dust devils are  
328 all larger than 10 m—suggesting that these too are “exceptional” events and again the more  
329 typical, smaller examples have not been detected.

330 Despite these caveats, the wind speeds within dust devils have been measured. Some au-  
331 thors have measured only the magnitude of the horizontal wind speeds within the dust devils,  
332 whereas others have provided all three components (i.e. inflow, tangential and vertical wind  
333 speed). Speeds are usually quoted at a height of 2 m above the ground, but measurements  
334 both nearer the ground (e.g. Balme et al. 2003) and higher into the dust devil (e.g. Kaimal  
335 and Bussinger 1970) have been reported. The following key points have emerged: (i) the  
336 horizontal winds within dust devils can often reach  $10 \text{ m s}^{-1}$  (e.g., Ryan and Carroll 1970),  
337 can peak at  $> 25 \text{ m s}^{-1}$ , but rarely, if ever, exceed  $30 \text{ m s}^{-1}$  (see Balme and Greeley 2006,  
338 Table 4, and Lorenz 2016, Table 1), (ii) vertical wind speeds are usually a factor of several  
339 less than the horizontal winds (e.g., Balme and Greeley 2006, Table 4), (iii) larger dust  
340 devils appear to contain stronger swirling winds, but vertical wind speeds do not correlate  
341 with diameter (e.g., Ryan and Carroll 1970), and (iv) the surface shear stress provided by  
342 the wind speeds within terrestrial dust devils appears sufficient to lift almost all sizes of  
343 naturally occurring loose sediments up to about granule-sized material (Balme et al. 2003).

### 344 2.1.5 Dust Load

345  
346  
347 Due to the fast-changing environment within dust devils, the concentrations of airborne dust  
348 and larger particles within dust devils are difficult to measure. The most complete study of  
349 particle loading in dust devils is that of Metzger et al. (2011), who used in-situ sampling  
350

351 on a mobile platform. Few other studies exist for terrestrial dust devils: a preliminary LI-  
352 DAR observation at 100 m height (Renno et al. 2004) provided an estimate of dust load of  
353  $\sim 100 \text{ mg m}^{-3}$  and there are reports of aircraft in-situ sampling of dust devils at 140 and  
354 300 m height (Gillette and Sinclair 1990), but only flux data are given, not particle load.  
355 Other datasets exist for martian dust devils (e.g. Greeley et al. 2006, 2010), but Metzger  
356 et al. (2011) provide the main source of dust load data for Earth.

357 Metzger et al. (2011) present data from more than 30 encounters at two field sites and  
358 over four field seasons. They used both PM-10 sensors (sensitive to dust grade materials,  
359 0.1–10  $\mu\text{m}$  diameter) and total suspended load sensors (dust- to sand-grade materials). All  
360 measurements were made at the base of the dust devil (sensors were generally at 2 m height,  
361 but some measurements at 1, 2.8 and 4.5 m height are reported). They found that PM10 dust  
362 load had high intra- and inter-dust devil variability. In many cases they report both maximum  
363 and mean dust load per dust devil (rather than just reporting the peak dust load) and report  
364 a peak range of 6–162  $\text{mg m}^{-3}$  and mean range of 0.8–42  $\text{mg m}^{-3}$ . The measured total  
365 suspended particle load (i.e. including larger sediments) was much higher: ranging from  
366 6–875  $\text{mg m}^{-3}$ . Metzger et al. (2011) conclude that mean peak dust load (i.e. the amount of  
367 dust likely to lofted to height by a dust devil) is about three times less than the peak load  
368 measured, and that the total suspended particle load near the base of the dust devil is about  
369 ten time greater than the PM-10 fraction. They note, however, that the larger size fraction  
370 material is unlikely to be transported to great height, and is probably redeposited locally.  
371 This measurement is in agreement with observations of a “sand skirt” at the base of many  
372 dust devils. Oke et al. (2007) measured particle size within the bottom  $\sim 1.5$  meters of willy-  
373 willies, finding that sand sized particles were confined below  $\sim 20$  centimeters. Raack et al.  
374 (2014) find similar results in Morocco.

### 375 2.1.6 Seasonal and Diurnal Frequency of Occurrence

376  
377  
378 As they are convective vortices, driven primarily insolation, dust devils occur most fre-  
379 quently when there is strong, continuous sunshine. This is usually in the summer, but they  
380 can occur at any time of year when there is a significant thermal contrast between the ground  
381 and the atmosphere (for example, dust devils have been seen in the Canadian sub-arctic;  
382 Grant 1949). To our knowledge, no season-to-season monitoring of dust devil activity has  
383 been performed to further refine the seasonal frequency, though.

384 In terms of diurnal rate of occurrence, many authors have noted that dust devils form  
385 most frequently in the late morning and the early afternoon (see summary by Balme and  
386 Greeley 2006 and recent work by Kurgansky et al. 2011). However, many of these reports  
387 are based on observer surveys which are both qualitative and which are unlikely to have run  
388 throughout the day—so there is always a possibility of bias. Recent work by Lorenz and  
389 Lanagan (2014) using a continuous month-long survey of pressure excursions to detect dust  
390 devils showed that most dust devils occur between 10:00 and 16:00 local time. They do note  
391 that about 10 % of the day’s dust devil events occur after 16:00 and there is a measurable  
392 tail of activity even after 18:00.

393 Several authors note that dust devil events are ‘clustered’ in time, with periods of more  
394 intense activity separated by periods of less activity. Carroll and Ryan (1970) suggest a  
395 periodicity of around 45 minutes and Renno et al. (2004) a periodicity of about 20 minutes.  
396 Lorenz and Lanagan’s (2014) pressure-excursion data hint at a similar result.

397 In addition to surveys by human observers making either continuous records or recording  
398 at intervals (e.g. how many are seen at 15-minute intervals), the availability of time-lapse  
399 cameras, webcams etc. now allow new surveys with superior temporal coverage, and with  
400

quantitative detection criteria (e.g. optical contrast of 1 %). It is important in all such surveys that the detection criterion (size, contrast), and measurement cadence be documented—for instance images acquired at a given cadence or observing distance may preferentially detect a particular size of dust devils (Lorenz 2011; Kurgansky et al. 2011).

### 2.1.7 Thermal Imaging

The warm core of a dust devil and/or its suspended dust warmed by insolation absorption would be expected to provide a radiative thermal signature. Lorenz (2004) provided the apparent first scientific report of thermal infrared imaging of a dust devil (although Metzger et al. 2010, have since reported thermal imaging of Atacama dust devils, and Towner 2008, report orbital thermal imaging of dust devils at Mars). Thermal imagers have reduced significantly in cost in recent years, in part due to application in home improvement (to detect damp or poor insulation in walls). An example image is shown in Fig. 2.

The Lorenz (2004) observation reported a single dust devil as it moved away from an initial distance of 10 meters. The vortex temperature of 38–40 °C derived from the 8–14 μm emission was approximately the same as the measured ambient air temperature but greater than the background atmospheric ‘brightness’ temperature of 12–20 °C obtained for lines of sight that did not intersect the dust devil. Lorenz (2004) noted that the dust might even be physically warmer than the surrounding air due to its interception of sunlight, a factor that might enhance the intensity of a vortex when dust is lifted (as later discussed by Fuerstenau 2006). Thermal imaging might provide a higher-sensitivity means of detecting marginally visible dust devils under some circumstances (notably, low-light levels) but this has not been robustly demonstrated. It may be that thermal imaging could also help visualize the near-surface wind stress field around the devil (e.g. showing ‘spiral’ arms of the inflow, as can sometimes be seen on the ruffled surface of the sea around waterspouts) due to the wind-dependence of surface heat transfer.

## 2.2 Remotely Imaged Martian Dust Devil Characteristics

The opportunities for martian surface-based acquisition of visible imaging and subsequent characterization of dust devils has been limited to the two Viking Landers (1976–1982), Mars Pathfinder (1997), Mars Exploration Rovers Spirit (2004–2010) and Opportunity (2004–present), Phoenix Lander (2008), and Mars Science Laboratory Curiosity Rover (2012–present). Some of these missions provided no visible evidence of dust devil occurrence (Viking), while others provided the current best martian dust devil climatology (*Spirit*). Because imaging observations are discretely separated between robotic missions, we follow a chronological mission order presentation below.

A summary of observations is presented in Table 2.

### 2.2.1 Viking Lander & Mars Pathfinder Imaging

The two Viking Landers safely settled onto Mars’ surface during 1976, at subtropical (VL1) and middle (VL2) northern latitudes. VL1 returned measurements spanning 2245 sols covering portions of four martian years, while VL2 returned measurements for 1050 sols. Despite the substantial temporal extent of the Viking lander imaging data sets, these landers were unable to image dust devils because their cameras were facsimile-type imagers not well-suited to detecting moving objects (Lorenz et al. 2016). As a consequence of this characteristic of the Viking camera system, the first opportunity to visually detect martian dust devils from a

**Table 2** Martian dust devil observed characteristics

| Parameter                                     | Best observations or measurements   | Key literature  |
|---|---|---|
| Size (diameter)                               | Inferred core diameters 10–700 meters from Viking wind measurements (not visually confirmed); 15–550 m (most frequent 100–200 m) from Pathfinder IMP (for assumed $10 \text{ m s}^{-1}$ translation speed); median diameter 20–40 m from Spirit Nav Cam; MSL pressures and winds (16 m median; 21 meter mean) | Ryan and Lucich (1983); Ringrose et al. (2003); Ferri et al. (2003); Greeley et al. (2010); Kahanpää et al. (2016)                            |
| Size (height)                                 | ~ 10–400 m (though many images truncate vortex top); maximum verified lower limit ~ 800 m   | Greeley et al. (2006)   |
| Lifetime/Detection Duration                   | 120–180 seconds from imaging; wind effect determination duration (60–1000 seconds); FWHM from wind pressure measurements (5–20 seconds)   | Ringrose et al. (2003); Ferri et al. (2003); Greeley et al. (2010); Ellehoj et al. (2010); Kahanpää et al. (2016); Steakley and Murphy (2016) |
| Morphology                                    | Columnar, disordered or v-shaped; few columnar vortices include a v-shaped ‘sand skirt’   | Greeley et al. (2006); Ferri et al. (2003)  |
| Rotation sense                                | Equally clockwise and counter-clockwise   | Ryan and Lucich (1983)  |
| Wind speeds (peak horizontal) at ~ 2 m height | Maximum measured speeds are ~ $30\text{--}40 \text{ m s}^{-1}$ ; maximum inferred core boundary speeds approach $100 \text{ m s}^{-1}$ for two instances which correspond with the greatest spatial extrapolation to that core boundary position  | Ryan and Lucich (1983); Ringrose et al. (2003); Ellehoj et al. (2010)   |
| Wind speeds (peak vertical) from imaging      | Maximum ~ $17 \text{ m s}^{-1}$ , with median $1.0\text{--}1.6 \text{ m s}^{-1}$  | Greeley et al. (2010)   |
| Horizontal translation speed                  | A few to ~ $25 \text{ m s}^{-1}$ (median ~ $2 \text{ m s}^{-1}$ ) (Note: ambient wind speeds were not correspondingly available)  | Greeley et al. (2010)   |
| Dust loading                                  | $700 \text{ mg m}^{-2}$ for a horizontal path through a dust devil, implying $20 \text{ mg m}^{-3}$ for a 35-m diameter dust devil, for Pathfinder; $0.002\text{--}250 \text{ mg m}^{-3}$ for Spirit; coarse particles (> 63 micrometers) confined to < 30 cm above the surface                               | Metzger et al. (1999); Greeley et al. (2010); Oke et al. (2007)   |
| Temperature excursion                         | Measured excursions of 1–6 °C for Viking & Pathfinder & Phoenix; MSL/REMS   | Ryan and Lucich (1983); Murphy and Nelli (2002); Ringrose et al. (2003); Ellehoj et al. (2010); Kahanpää et al. (2016)                        |
| Core pressure excursion ( $\Delta P$ )        | 0.3 to ~ 5 Pa; lower limit arises from limit imposed upon the analyses, with smaller magnitudes more frequent; no measurement regarding verified vortex maximum $\Delta P$ excursion is available   | Murphy and Nelli (2002); Ellehoj et al. (2010); Kahanpää et al. (2016); Steakley and Murphy (2016)  |
| Electric fields                               | No measurements available   |   |

surface vantage point occurred with the Mars Pathfinder Lander (MPF) mission. It is tempting to speculate that the facsimile-type imager on the Viking landers may have a few dark lines in parts of a few images caused by dust devil passages during their slow scans, but these would be challenging to detect and attribute.

MPF began operation on Mars' surface on 04 July, 1997 in the northern subtropical (19.3 N, 33.4 W; Golombek et al. 1997) Ares Vallis region located  $\sim 1000$  kilometers east-southeast of Viking Lander 1. The mission provided measurements spanning 83 sols covering the latter third of northern summer through very early northern autumn ( $L_s$  142–183). There was some expectation that Pathfinder would have the opportunity to detect dust devil signatures within its meteorology (MET) measurements (Seiff et al. 1997).

From analysis of multi-color images provided by the Imager for Mars Pathfinder (IMP) (Smith et al. 1997), Metzger et al. (1999) reported the first identification of martian dust plumes within surface-obtained images. Image enhancement via band subtraction was employed to isolate the low-contrast signature of the dust plume. Dust plumes were most evident as occultation features at blue (430 nm) wavelengths among the Imager for Mars Pathfinder (IMP) wavelength filters, which also included 530 and 670 nm, due to the reduced dust scattering at that shorter wavelength. Five dust plumes were identified within 16 analyzed IMP images obtained near mid-sol on sols 10 and 11 of the 83-sol mission when landing site panoramas were being acquired. Dust devil diameter (14–79 meter) and height (46–450 meters) and translation speed ( $0.5\text{--}4.6\text{ m s}^{-1}$ ) were estimated from the angular width and motion derived from multiple images and the inferred distance from the lander obtained from identification of foreground and background features. The plume/vortex dust load ( $\sim 7 \times 10^{-5}\text{ kg m}^{-3}$ ) was estimated to be  $\sim 10,000$  times greater than the background dust load.

Ferri et al. (2003) applied the Metzger et al. (1999) band subtraction technique to a more extensive set of horizon-containing IMP images and identified 14 dust plumes/devils that included the 5 from Metzger et al. (1999). Only one of these identifications occurred for an image that was not part of the panorama captured during mission sols 10–11. To quantify vortex size, a constant translation speed of  $10\text{ m s}^{-1}$  was assumed, with the observed angular rate of motion from consecutive images being employed to estimate vortex distance and subsequently vortex size. The 14 identified vortices were estimated to span the size range of 10–570 meters and to have been positioned 1–25 km from the lander. A surface vortex surface area coverage of  $2 \times 10^{-4}$  (0.02 %) was estimated for the 0900–1500 local true solar time (LTST) time interval. This fractional coverage, coupled with a derived vortex vertical dust flux estimate of  $7 \times 10^{-5}\text{ kg m}^{-2}\text{ s}^{-1}$ , resulted in an estimated total vortex-induced vertical dust flux of  $3.6 \times 10^{-9}\text{ kg m}^{-2}\text{ s}^{-1}$ , which exceeded by an order of magnitude the estimated local dust deposition rate (Landis and Jenkins 2000).

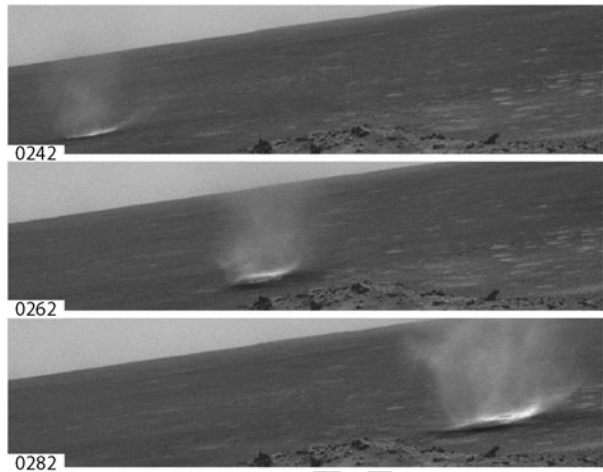
In addition to images, one IMP-provided opacity measurement from direct solar imaging on sol 14 resulted in larger values at all wavelengths compared to more than 10 additional opacity observations obtained that same sol (Smith and Lemmon 1999). This increased opacity event could possibly have been the result of a dust-laden vortex occulting the Sun but no additional supporting measurements, including contemporaneous MET measurements, are available.

Thus, the Pathfinder mission did verify that dust devils, or at least dust plumes (since motion within a plume was not identified), are visible from Mars' surface, but these imaging results did not provide a rigorous quantitative characterization of martian dust devils.

### 2.2.2 Mars Exploration Rovers (*Spirit* & *Opportunity*)

After the experience gained with the martian dust devils identified in the MPF IMP images, the Mars Exploration Rover (MER-A & B—*Spirit* & *Opportunity*) science teams prepared for the possibility of observing dust devils at the two landing sites: Gusev Crater (*Spirit*) and Meridiani Planum (*Opportunity*). MER science teams planned on using similar band-subtraction techniques for viewing dust devils as was originally used by Metzger

**Fig. 3** Three images from a typical *Spirit*—Navigation camera sequence used to create martian dust devil “movies”. Numbers in the lower left of each image indicate the number of seconds since the image sequence began. This sol 456 dust devil viewed from the west flank of the Columbia Hills translates from left to right, passing over a small bright toned depression as it moves



et al. (1999) to enhance the contrast to make these difficult phenomena easier to study. The Panorama Cameras (Pancam) on the MERs were higher resolution than the Imager for Mars Pathfinder (IMP) and capable of better images, but it was not known if either of the two locations would be capable of producing better, more visible dust devils than those observed in Ares Vallis with MPF. Orbital images suggested that Gusev Crater (*Spirit*) would have a good chance of seeing dust devils because of a swath of features across the crater with many dust devil tracks (Greeley et al. 2003). However, prior to *Spirit*'s landing, active dust devils had not been observed from orbit in Gusev crater, casting doubt that the swath of dark features were in fact dust devil tracks. *Spirit* landed near the end of Southern Hemisphere Summer ( $\sim L_s$  330) [Squyres et al. 2004]. The first part of the mission produced no imaging-detected dust devils at either location for the rovers, and many searches through images using the band subtraction technique yielded no results (Lemmon et al. 2004), although one new dust devil track was observed from orbit, having formed between  $L_s$  12 and 22 (Lemmon et al. 2015). On sol 421 ( $L_s$  173), while *Spirit* was perched on the Columbia Hills near the center of the Gusev, the first dust devil was observed, differing greatly from the nebulous wisps from the MPF images. The MER image was crisp and detailed and as with subsequent observations, the dust devils were clearly visible as distinct from the background (Fig. 3). Observations at Meridiani by *Opportunity* have been limited to a few sightings of individual dust devils that could be a result of poorer viewing geometry and/or limited liftable dust (Lemmon et al. 2015).

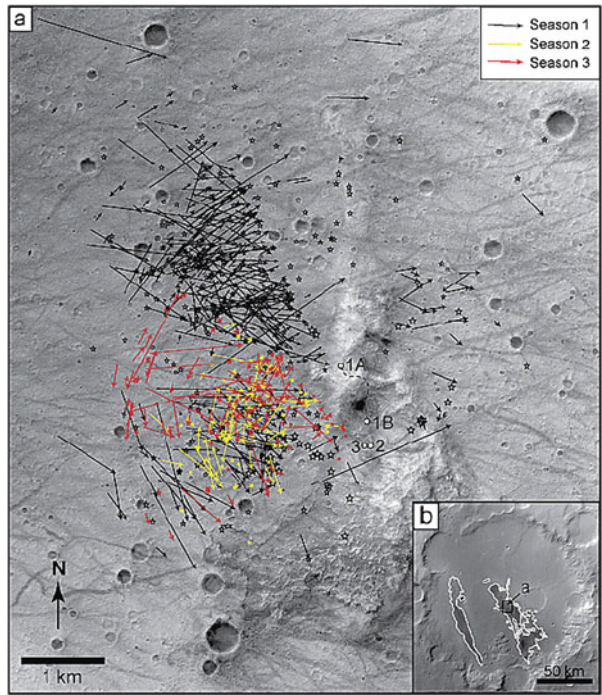
After the first year of the mission, an elevated vantage point on Husband Hill offered several advantages over the previous lander geometry (Greeley et al. 2006). Sitting above the plains of the crater floor, the dust devils appeared bright against the ground, and darker against the sky above the horizon. The elevated viewing angle also allowed each dust devil to be more precisely located against surface features such as smaller craters and hollows, and rock patterns. More precise locations allowed better distances to be known, allowing for better estimations of sizes. Once the first dust devil season officially started, it became clear that dust devils could be seen easily in all of the rover's camera systems including not only the Pancam, but also the lower resolution monochrome Navigation Camera (Navcam) and both the forward and rear Hazard Cameras (Hazcams). Specific imaging campaigns were designed to make use of what was known about dust devil statistics. Initial dedicated imaging occurred during  $\sim$  0900–1700 LST. Subsequently, Navcam and Pancam images

601 were subframed upon the ground/sky boundary and the most common locales for dust devil  
602 occurrence. Subframing reduced the amount of storage space for each image and allowed  
603 multiple image, “movie”, sequences to be obtained (Fig. 3). The  $\sim 20$  second frame rate on  
604 the movie sequences was limited by the refresh rate of the cameras’ CCDs and the image  
605 buffer, but the image acquisition times refresh cycle was well known, allowing time between  
606 frames to be accurately established. Due to the favorable viewing geometry, on many sols  
607 not only sizes of and distances to the dust devils could be determined, but also translation  
608 speeds (horizontal) of the dust devils suggesting background ambient wind speeds in Gusev.  
609 In some movie sequences, detail was high enough that pockets of dust from some of the hol-  
610 lows could be followed from frame to frame allowing rough estimates of vertical velocities  
611 to be determined.

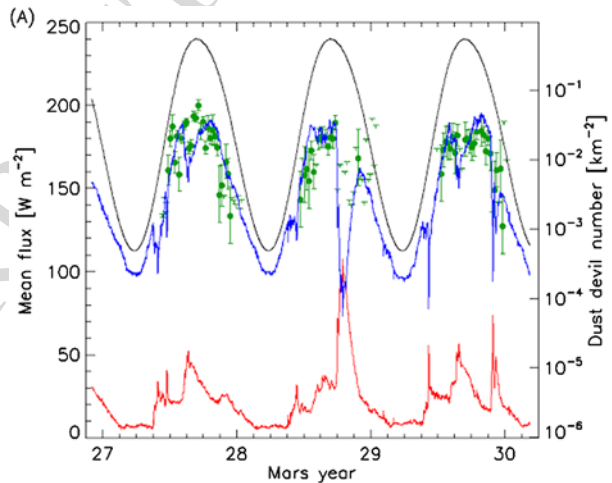
612 The longevity of the MER campaigns allowed for repeat seasonal studies of dust devil  
613 activity, which was particularly useful in Gusev Crater. *Spirit* had observed  $\sim 533$  dust  
614 devils in the first documented dust devil season (Greeley et al. 2006). This high number of  
615 individual vortices was due in part to excellent viewing geometry from atop the Columbia  
616 Hills, from where much more of the crater floor of Gusev was visible. As *Spirit*’s traverse  
617 led it further south into the saddle and eventually to the “Home Plate” feature, *Spirit*’s view  
618 of the crater floor was obstructed by the hills. Greeley et al. (2010) describes the three  
619 total observed seasons in detail. The second dust devil season began on about sol 1101  
620 ( $L_s$  181°), which was comparable to the first season’s start around sol 421 ( $L_s$  173.2°).  
621 The second dust devil season was truncated by the onset of a set of planet-encircling dust  
622 storms that restricted insolation at the surface, presumably prohibiting the formation of dust  
623 devils while the background atmospheric dust opacity rose to a peak tau of 4.31 (Greeley  
624 et al. 2010; Lemmon et al. 2015). While the dust opacity was so high, solar power for  
625 rover operations was limited and fewer images were taken, but of the images that were  
626 acquired, no dust devils were observed during the dust storm and the upper limit for dust  
627 devil frequency was an order of magnitude below pre-storm levels (Lemmon et al. 2015).  
628 The second season, with limited viewing geometry and the presence of strong regional dust  
629 storms, produced an observed 101 individually identified dust devils. The following martian  
630 year, 127 more vortices were observed when the third dust devil season began around sol  
631 1785 ( $L_s$  189°). Still located near Home Plate, *Spirit*’s view of the plains was still restricted  
632 similarly to the second season (Fig. 4). Over three Mars years, Lemmon et al. (2015) found  
633 that changes in dust devil frequency correlated with changes in surface insolation, whether  
634 the changes were seasonal or from dust storms, and that dust devil frequency fell to  $1/e$   
635 with each  $18 \text{ W m}^{-2}$  reduction in mean insolation (roughly 10 % of the peak insolation)  
636 (Fig. 5).

637 *Spirit* and *Opportunity* were not equipped with meteorological instrument packages for  
638 temperature and pressure measurements, but over the three dust devil seasons recorded  
639 at Gusev, several key measurements were made using the camera systems. For the first  
640 time on Mars there was repeat coverage at the same site for dust devil seasonal infor-  
641 mation. Correcting for sample bias, Greeley et al. (2010) estimated that the diurnal dis-  
642 tribution of dust devils at Gusev began after 0900 and tailed off before 1700 LTST. This  
643 time range was consistent for all three seasons at Gusev (Fig. 6). Peak activity occurred  
644 around 1300 LTST with some indication of possible burst of activity near the end of the  
645 day between 1400 and 1600 LTST. Tracking dust devils within movie sequences yielded  
646 estimates of both translational and vertical velocities. Translational speeds, which could  
647 serve as a rough surrogate to the background boundary layer winds across Gusev Crater  
648 were estimated to be between a few meters per second up to  $\sim 27 \text{ m s}^{-1}$  and maximum ve-  
649 locities tended to occur near the end of local springtime. Minimum vertical wind speeds  
650

651 **Fig. 4** (After Greeley et al.  
652 2010) Three seasons of dust devil  
653 occurrence locations within  
654 Gusev Crater. (a) Mosaic of  
655 HiRISE images of Spirit's  
656 operation area, with vectors  
657 indicating dust devil tracks from  
658 Spirit Navigation camera  
659 "movies", color coded for each  
660 season (year); stars indicate  
661 locations of active dust devils  
662 from single frames. (b) Mars  
663 Orbiter Camera Wide Angle red  
664 image R21-00168 inset of Gusev  
665 Crater showing the Gusev Low  
666 Albdeo Zone (GLAZ, outlined)  
667 where dust devil tracks are  
668 observed, and the location of  
669 Fig. 4a



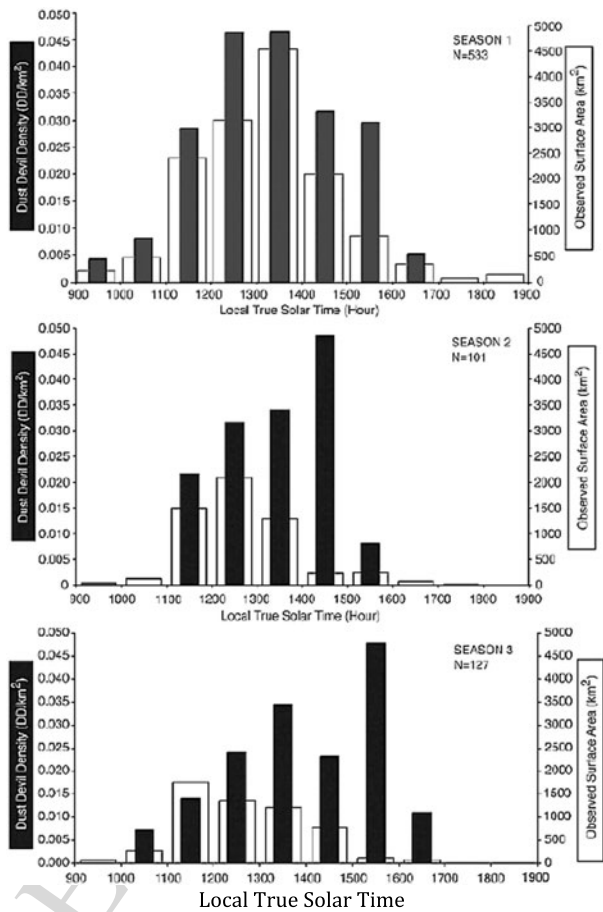
676 **Fig. 5** Insolation at the Spirit  
677 rover site. The continuous curve  
678 shows the modeled  
679 top-of-atmosphere, sol average  
680 insolation (upper, black), direct  
681 plus diffuse surface insolation  
682 (middle, blue) and atmospheric  
683 absorption of sunlight (lower,  
684 red). Symbols (green) show dust  
685 devil number density (right axis)  
686 reported by Greeley et al. (2010)  
687 with the T symbols indicating  
688 upper limits. (For the  
689 interpretation of the references to  
690 color in this figure legend, the  
691 reader is referred to the web  
692 version of this article)



694 within a few dust devil columns were estimated based on visual identification of small  
695 clumps of dusty material present from frame to frame in the movie sequences. Vertical  
696 wind speeds were estimated to be 0.04 up to  $\sim 17 \text{ m s}^{-1}$  with medians being between 1.0  
697 and  $1.6 \text{ m s}^{-1}$ . The data from the MER rovers, and Spirit in particular provide the most  
698 complete observation of a dust devil season on Mars and rival any campaign attempted on  
699 Earth.

## Field Measurements of Terrestrial and Martian Dust Devils

**Fig. 6** (After Greeley et al. 2010) Number density of Spirit observed dust devils versus Local True Solar Time (LTST) for three seasons (years).  $N$  is the total number of dust devils observed each season

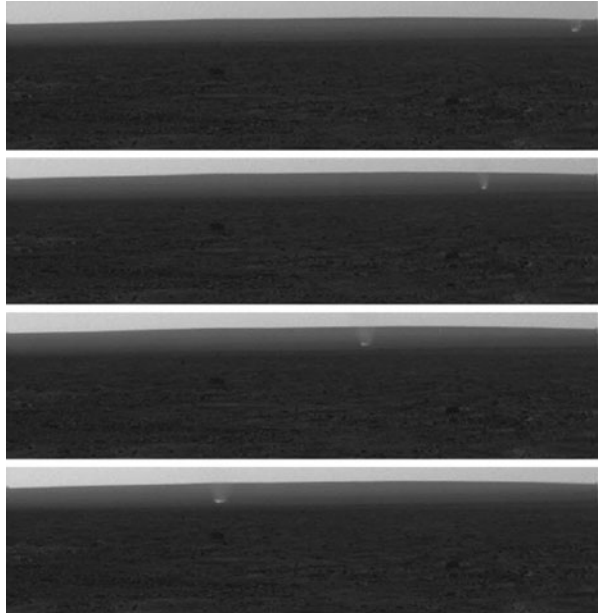


### 2.2.3 Mars Phoenix Lander

NASA's Mars Phoenix spacecraft (Smith et al. 2008, 2009) landed at an arctic location (68.2 °N, 234.3 °E) in the Martian Northern Plains on 25 May 2008, in early northern hemisphere summer ( $L_s$  77°). The primary mission lasted for 90 sols; contact was lost after 151 sols (circa 5 months), in late summer ( $L_s$  148°). Equipped with the Surface Stereo Imager (SSI), with adequate resolution to image dust devils, and a high-resolution pressure sensor, Phoenix became the second Mars lander, after Pathfinder, that had the capacity to detect dust devils both visually and by meteorological measurements. It was, however, not until sol 104 ( $L_s = 125^\circ$ ) that the first dust devil was spotted by SSI (Ellehoj et al. 2010). However, there had not been many opportunities to detect dust devils before this. Besides imaging geological targets close to the lander, this camera was used to monitor the Telltale wind indicator (Holstein-Rathlou et al. 2010). The first dust devil was detected serendipitously while imaging a panorama. After this first detection, Phoenix was commanded to take image sets aimed to search for dust devils. These sets consisted of 13 to 50 sequential images of the horizon.

Ellehoj et al. (2010) investigated the images taken by Phoenix of dust devils. Image contrast was enhanced, as had been previously done with the Pathfinder (Metzger et al. 1999;

**Fig. 7** This two-minute and 37-second time sequence (top-to-bottom) of contrast-enhanced Phoenix SSI images shows the translation of a mid-afternoon dust devil seen southwest of the lander on the mission's 109th sol ( $L_s = 127$ )



Ferri et al. 2003) and MER images (Greeley et al. 2006, 2010), allowing the detection of features with only an approximately 3 % difference compared to background albedo. 37 individual dust devils were identified in the SSI images obtained between sol 104 and sol 138 ( $L_s = 125\text{--}142$ ) (Fig. 7). The beginning and end of the Phoenix “dust devil season” could not be determined because the dust devil imaging campaign lasted only for a small fraction of the Martian year. However, the first Phoenix observations of dust devils were shortly (14 sols) after the Sun set for the first time in the mission—still near peak northern summer insolation, as at Gusev crater for southern summer, but when temperature contrasts could develop through diurnal cycles. The diurnal time range of SSI dust devil observations spanned 11:00 to 16:00 LTST, matching results of MER Spirit and the timing of vortices detected by the Phoenix pressure sensor (Sect. 3), although no dust devil search imaging was performed in the morning hours before 11:00 due to operational constraints on available energy to heat and aim the camera for use.

All dust devils were seen in the southwest direction, despite two-thirds of the horizon images having been obtained from other directions, with unobstructed views in all azimuths. The distances of the dust devils from the lander could not be determined in the featureless landscape so their physical size could not be evaluated. In most cases the dust devil was visible in several sequential images and was thus seen to move across the frame. As the distances were unknown, translation speeds could not be assessed. In most cases the direction of motion had an eastward component, agreeing with the wind directions measured by the Telltale wind indicator and orbital observations of dust devils and their tracks in the same area (Holstein-Rathlou et al. 2010; Reiss et al. 2014). The dust devils detected by Phoenix were too faint to enable determination of vertical wind speeds as had been done for some of the dust devils imaged by MER Spirit (Ellehoj et al. 2010).

## 2.2.4 Mars Science Laboratory/Curiosity Rover

The US/NASA Mars Science Laboratory (MSL) Curiosity rover has performed meteorological measurements since August 2012 in 154 kilometer diameter Gale crater, centered just south of the Martian equator (4.6 °S, 137.4 °E). Studying the modern Martian environment is one of the science goals of NASA's Mars Science Laboratory (MSL) mission (Grotzinger et al. 2012). MSL is, unlike the MERs, equipped with a meteorological station, a video-capable color science camera, and a MER-like high signal-to-noise navigation camera system with a reasonably high frame rate. With this payload and a planned operational lifetime of more than one Martian year, MSL could have become an almost perfect lander for the study of dust devils. However, the landing site in Gale crater turned out to be less than ideal for this purpose.

Prior to MSL's landing it was expected that very few, if any, dust devils would occur at this site. No dust devil tracks had been seen in orbital images of the crater floor (Fred Calef, Jet Propulsion Laboratory/Caltech, personal communication, 2012). Further, atmospheric modeling (Tyler and Barnes 2013; 2015) suggested that the depth of the daytime boundary layer inside the crater is suppressed. This suppressed, shallow depth was expected to reduce vortex activity, or at least vortex intensity, since the thermodynamic efficiency of vortices depends upon the boundary layer depth according to the so-called heat engine model (Renno et al. 1998, 2000). Nevertheless, an extensive campaign of imaging Dust Devil Search Movies was initiated after MSL's landing (Moores et al. 2015). The Dust Devil Search Movies are taken using MSL's monochrome Navigation Cameras (Navcam) and consist of four to eight frames with the central elevation on the horizon. All together 91 Dust Devil Search Movies were imaged during the first 360 sols of the mission. The result matched the expectations: only one very faint dust devil was detected on sol 41 ( $L_s = 173$ ). This virtual non-detection, combined with MSL's meteorological measurements, can be used to constrain the conditions where dust devils can form on Mars (Kahanpää et al. 2016; Klose et al. 2016).

Collectively, five spacecraft equipped with cameras suitable for imaging moving objects have landed on Mars: Mars Pathfinder, MER Spirit, MER Opportunity, Mars Phoenix and MSL. Despite the different landing sites, spanning latitudes from 14.6 °S (Spirit) to 68.2 °N (Phoenix), all of these landers have succeeded in imaging dust devils (or at least dust plumes), indicating that dust devils occur on all latitudes on Mars. While the other landers have imaged from tens to hundreds of dust devils, MER Opportunity and MSL have observed only a few, in spite of the long durations of these missions and active search for dust devils, showing that there are strong variations in local dust devil occurrence rates.

While martian surface obtained imaging has provided direct evidence for dust devils, only the Spirit rover within Gusev Crater has provided measurements from which internal vortex characteristics have been quantified and then only minimally. The Spirit observations did provide valuable seasonal and time-of-sol occurrence characterization; Phoenix provided some seasonal indication of occurrence variation but the number of images available for analysis were more limited than the number and seasonal extent available from Spirit.

## 3 Surface Obtained Meteorology Measurements of Dust Devils

In addition to their visual manifestation, dust devils can also be characterized via in situ measurements of their thermodynamic conditions, including the central pressure drop, wind speed, temperature, suspended dust load, surface dust lifting magnitude, electrostatic state,

etc. For such measurements to be of statistical characterization value, high sampling frequency and long duration (seasonal, annual) measurements are best, but until recently such long lived measurement opportunities were not the norm. Previous in situ measurements have provided much of the knowledge currently available regarding dust devil thermodynamics. Despite their often incomplete coverage and potential biases these measurements are the foundation upon which current and future measurements of terrestrial dust devils are constructed.

A compilation of measured characteristics is provided in Table 1.

### 3.1 Meteorological Measurements of Terrestrial Dust Devils

Sporadic serendipitous meteorological encounters with dust devils were reported in the early literature, such as an encounter with the barograph at a small airport (Wyett 1954) but the first systematic measurements began in the 1960s. A particular challenge is that dust devil phenomena generally occur on timescales (seconds) that require fast instrument response and data acquisition. Sinclair (1966) made pressure, temperature and wind measurements with a hand-carried recording instrument station, and later a more elaborate station mounted on a jeep. The mobile sensor platform allowed penetration of dust devils within a reasonably short ‘hunting’ season, and data acquisition arrangements included a cine camera recording instrument readings.

Also in the 1960s, two sets of fixed-station investigations were performed. Lambeth (1966) set up an array of 6 meteorology stations at White Sands Missile Range, and recorded (with chart recorders) 19 encounters in a several month period. This rather low encounter rate proved discouraging, leading the author to recommend vehicle-borne measurements. On the other hand, Ryan and Carroll (1970) made temperature and wind measurements at a single fixed mast in the Mojave desert, but groomed the ground around the mast to ensure dust availability.

Field studies of dust devils saw a renaissance in the late 1990s and early 2000s with the observation of dust devils on Mars by Mars Pathfinder (Sects. 2b, 3b), and the prospects for observing more there with a lander planned for 2001 (later cancelled) and by Beagle 2. These impending Mars missions lead to several field campaigns in Arizona and Nevada (e.g. Tratt et al. 2003; Ringrose et al. 2003; Renno et al. 2004; etc.) during which, again, the measurements were principally vehicle-borne.

The presentation below of terrestrial dust devil measurements follows a measured parameter structure, with emphasis upon more recent measurements.

#### 3.1.1 Pressure Measurements

While providing a time-efficient means of acquiring measurements in dust devils, vehicle-borne chase measurements do not reproduce how measurements are acquired on Mars, where a single fixed station records data over an extended time, but not continuously. In addition to vehicle disturbance of measurements (e.g. visible in Tratt et al. 2003) and often rather poorly-documented distance histories, the tendency to chase the biggest, slowest devils leads to strong selection biases, which make it difficult to estimate the characteristics of the dust devil population. Technological developments in flash memory in the late 2000s allowed inexpensive data acquisition (Lorenz 2012b) with compact and low-power systems that could be deployed for months, sampling at  $> 1$  Hz without requiring operator visits to download data or replace power supplies. Furthermore, when only pressure and light levels are recorded, the logging package can be placed in

## Field Measurements of Terrestrial and Martian Dust Devils



**Fig. 8** Pressure and solar-flux logger used by Lorenz and Jackson (2015) and elsewhere. The commercial logger itself is essentially a USB memory stick (*green cylindrical object at lower right*) which can accommodate a single AA battery to operate for several days. Here a  $2 \times$  AA battery holder (which due to peculiarities of the power supply system yields about a month of operation at 2 Hz) is included, as well as a solar cell to record the shadow of dust devils. The whole unit can fit in a pocket. Note the logger identifier, necessary as these loggers have been installed in arrays

a box with a volume of less than 0.5 liters (Fig. 8) and simply set on the ground: this can be done in such a way (with a camouflaged housing) such that attrition by theft or vandalism at open sites is minimal. The systems are inexpensive enough ( $\sim$  \$150) compared with the cost of deployment and retrieval that they can be considered somewhat expendable. These systems have allowed large numbers (hundreds to thousands) of unperturbed vortex encounters to be obtained without chase biases, finally yielding robust statistics on vortex populations from pressure drops (Lorenz and Lanagan 2014; Jackson and Lorenz 2015) and on dust loading (Lorenz and Jackson 2015). Furthermore, the small measurement stations can be deployed in spatial arrays to make simultaneous measurements that resolve the two-dimensional horizontal structure of dust devils (Lorenz et al. 2015a, 2015b, 2015c).

The pressure loggers developed by Lorenz (2012a, 2012b) are compact enough that they can be easily carried in a pocket and operate without attention for many days, allowing opportunistic pressure measurements during other field activities without extensive preparation. For example, Lorenz and Radebaugh (2016) report the first in-situ measurements of vortex activity at a high-elevation site (a yardang and gravel-ripple field at 3800 m in the Argentinian Andes high plain—Puna) using such methods, indicating higher levels of dust devil activity than reported previously elsewhere (see also Chap. 8 of this volume, Lorenz et al. 2016).

Pressure drops associated with dust devils have been recorded opportunistically at a few sites (notably by chart-recording barographs as early as the 1950s—see Chap. 1 of this volume, Lorenz et al. 2016). A number of pressure traces were obtained in vehicle encounters by Sinclair (1969) and subsequent studies, but until recently, the pressure signatures of vortex encounters were better-documented at Mars (Lorenz 2012a) than on Earth. The ‘expendable’ small pressure loggers advanced by Lorenz (2012b) were deployed at Eldorado playa near Boulder City, NV, and showed promise. Three such loggers were operated for a one-month period in June 2012 (Lorenz and Lanagan 2014), generating the first statistically-robust terrestrial dataset of fixed-station encounters (and allowing comparison of their power-law statistics with those at Mars—see Lorenz et al. 2016, in this issue). Note

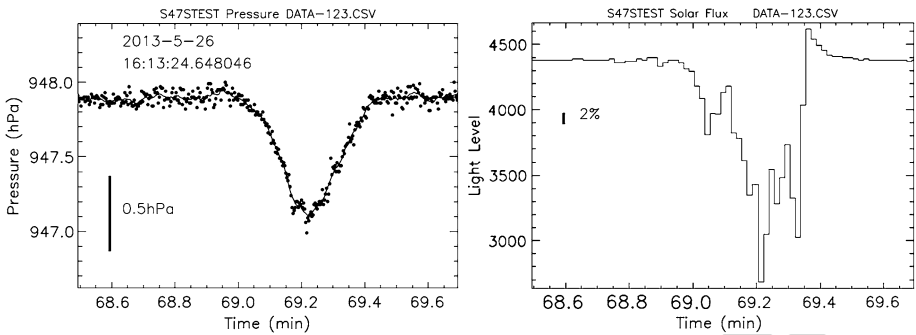


**Fig. 9** A solar logger encounter with a large dust devil on Eldorado in summer 2013 (from Lorenz and Jackson 2015). A broad pressure drop lasting about 20 s is seen; this pressure drop of about 0.7 mbar is typically encountered not more than once in a few weeks. The solar flux measurement at right shows that the devil was heavily dust-laden, blocking about 30 % of the light: the two prominent troughs are probably the wall of the dust column. Note that the light level \*rises\* after the encounter—part of the normally dark sky is occupied by dust which scatters light onto the solar cell in addition to the direct solar beam which is now no longer shadowed. This indicates the devil was moving away from the solar azimuth

that the recorded pressure drop at a point is a function of the vortex pressure field (related to diameter and intensity—see the companion chapter by Kurgansky et al. 2016) and the trajectory of the dust devil relative to the measurement station. Importantly, the data were made available for the use of other workers.

Jackson and Lorenz (2015) extended the Eldorado study with observations from several sites over summers 2012 and 2013, and the intervening winter, giving insights into the seasonal variation of vortex occurrence, and interannual variability (e.g. due to dust availability—flooding of the playa altering the surface texture and thus the lifting threshold—see Neakrase et al. 2016 in this issue). That study also explored automatic detection methodologies (finding over 1000 events), since these measurement approaches develop many Gigabytes of data, for which the manual vortex detection employed by Lorenz and Lanagan (2014) would have been prohibitive: the  $\sim 1200$  station-days of data comprise some 120 million measurements.

Lorenz and Jackson (2015) performed another study at 4 locations at Eldorado in summer 2013, using loggers with a solar cell to record dust devil shadows (Fig. 8). This study found that about half of pressure encounters were accompanied by measurable light level drops (Fig. 9). Some dustless vortices occurred, and in others, the devil's shadow missed the logger.

The Eldorado site is an open area, used for various recreational purposes, at which large unattended installations may encounter human interference (although artfully-concealed small loggers have been generally unaffected, although occasionally damaged by flooding). Lorenz et al. (2015b) employed another field site, La Jornada Experimental Range in New Mexico (operated by the US Department of Agriculture) where access is restricted and so larger installations can be left safely unattended.

This facility was used by Lorenz et al. (2015b) to deploy a line array of pressure/solar loggers in summer 2013. In addition to providing population statistics at this site, the survey noted that the number of vortices encountered varied quite substantially over a distance of a few tens of meters, due presumably to the influence of topography on dust devil migration and/or the effects of different scrub bushes on dust availability and surface roughness. This array study generated for the first time (since a pioneering chart-recorded 6-station study by

Lambeth 1966) simultaneous measurements exposing the horizontal pressure structure of dust devils. An example dataset is shown in Fig. 10, illustrating the radial variation of the measured pressure drop detected as the vortex passed across the pressure sensor array.

### 3.1.2 Wind

In a supplemental investigation to pressure logging, Lorenz (2016) obtained a high-quality set of wind speed and direction data at the Jornada Experimental Range in summer 2014, using the same logger technology as the Lorenz and Jackson (2015) effort. These data, uncontaminated by vehicle motion effects, allowed rather accurate vortex model fits, e.g. Fig. 11, wherein the pressure, wind speed and direction histories are simultaneously fit. The superposition of the circumferential vortex winds and the ambient wind field result in quite distinctive wind direction and speed histories, which resolve most of the geometric ambiguities intrinsic to fitting a pressure time series alone.

### 3.1.3 Other Terrestrial Dust Devil Observations

**Electric Fields/Saltation—Dust Flux** Dust on Earth is mainly lifted from the surface through the process of ‘saltation’ (Bagnold 1941; Shao 2008): when wind friction velocity/surface stress overcomes a threshold, its drag force causes larger particles with size around 100 micrometers to be the first to move. They jump over the surface, where they reimpact and initiate the motion of particles of a wide range of sizes, including dust. Indeed, due to dust sized particles protruding minimally upward into the wind affected near-surface atmosphere and also strong interparticle forces, dust grains are difficult to be lifted directly by the wind force (Gillette et al. 1974; Greeley and Iversen 1985; Shao et al. 1993).

The collisions among particles during saltation are also responsible for electric charge transfer between grains. Even if the exact mechanism for this process is still not clearly understood, some experiments and observations show that this process is size dependent (Freier 1960; Inoulet et al. 2006; Duff and Lacks 2008; Lowell and Truscott 1986; Kok and Renno 2008; Desch and Cuzzi 2000; Forward et al. 2009; Gill 1948; Latham 1964; Latham and Stow 1968; Harper 1967; Horn et al. 1993; Lacks and Levandovsky 2007). Considering that, in general, the smallest particles are transported higher into the atmosphere by local turbulence while larger particles remain closer to the surface, this translates in a charge separation and consequently in an enhancement of the atmospheric electric field.

So generally, a variation of the electrical properties of the atmosphere is observed during dust events including dust storm and dust devils with electric fields up to 150 kV/m being measured (Esposito et al. 2016a, 2016b; Schmidt et al. 1998; Renno et al. 2004; Kok and Renno 2006, 2008; Harper 1967). Fig. 12 shows an example of electric field observed during a dust devil (Esposito et al. 2016a, 2016b).

Esposito et al. (2016a, 2016b) undertook field test campaigns in the West Sahara desert to study dust lifting process by monitoring simultaneously weather parameters (pressure, wind, relative humidity, temperature, solar irradiance), soil properties (temperature, moisture), sand and dust dynamics (dust size distribution and abundance, sand saltation rate and flux), and the atmospheric electric field (with a field mill). They monitored several dust storms and devils. They found that there is a very strong correlation between the concentration of dust lifted during a dust storm and the atmospheric electric field intensity. The same behavior was observed also during dust devils, indicating that a similar dust electrification process was in action (Fig. 13).

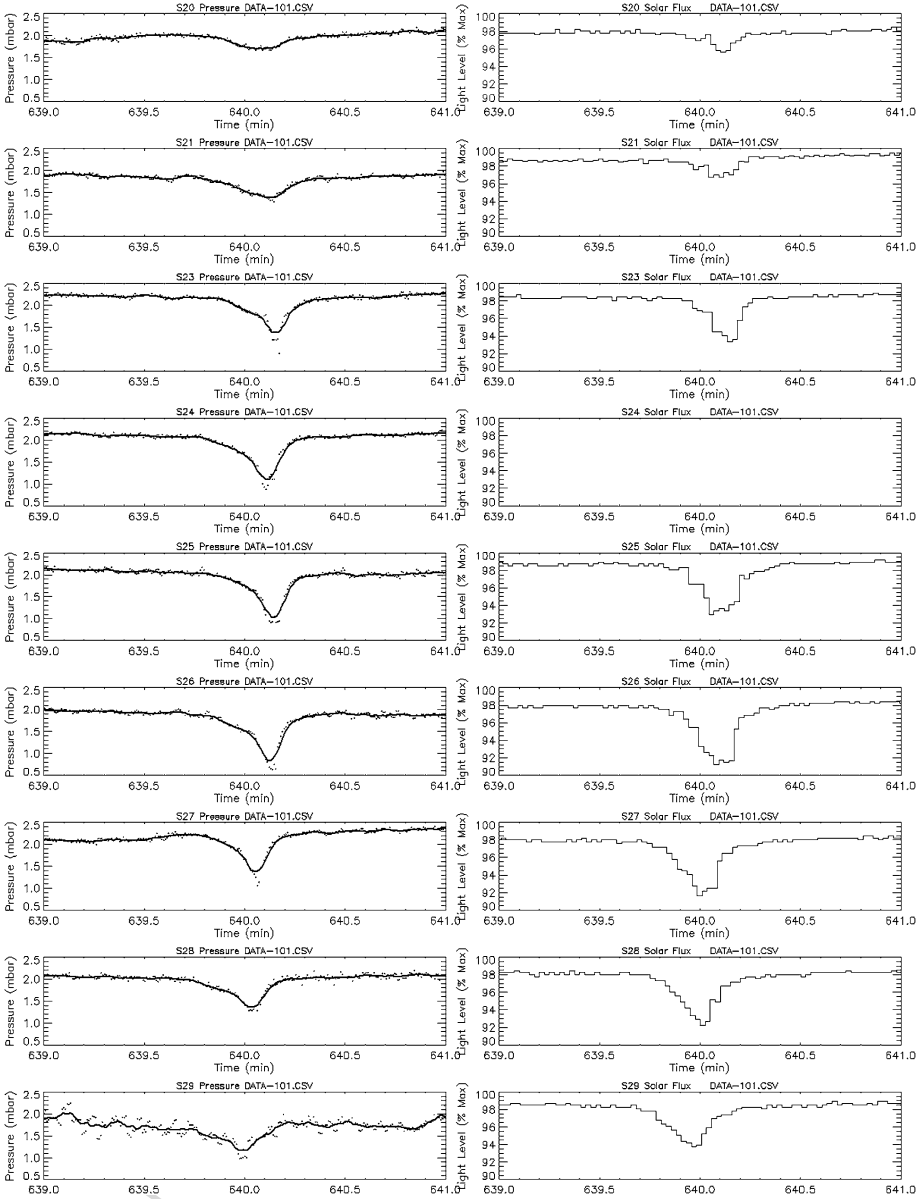


**Fig. 10** A ‘bullseye’ encounter at La Jornada, where a dust devil swept across a 10-station pressure/solar logger array. A signature is visible in all stations, but falls off in amplitude to either side. The plots are a 2-minute record from each station, with pressure (normalized to the beginning of the original datafile) plotted on the *left*, and solar flux (normalized to maximum) on the *right*. The devil is dust-laden, as evidenced by the sunlight drop that is simultaneous with the pressure signal. Note that no solar data is available on station S24 (which had been flipped over, perhaps by animal action). Note that the profile is asymmetric—the onset of the pressure drop is shallower and longer than the decay, a feature often seen and perhaps associated with the advection of the devil in the ambient wind field. [After Lorenz et al. 2015b]

Field Measurements of Terrestrial and Martian Dust Devils

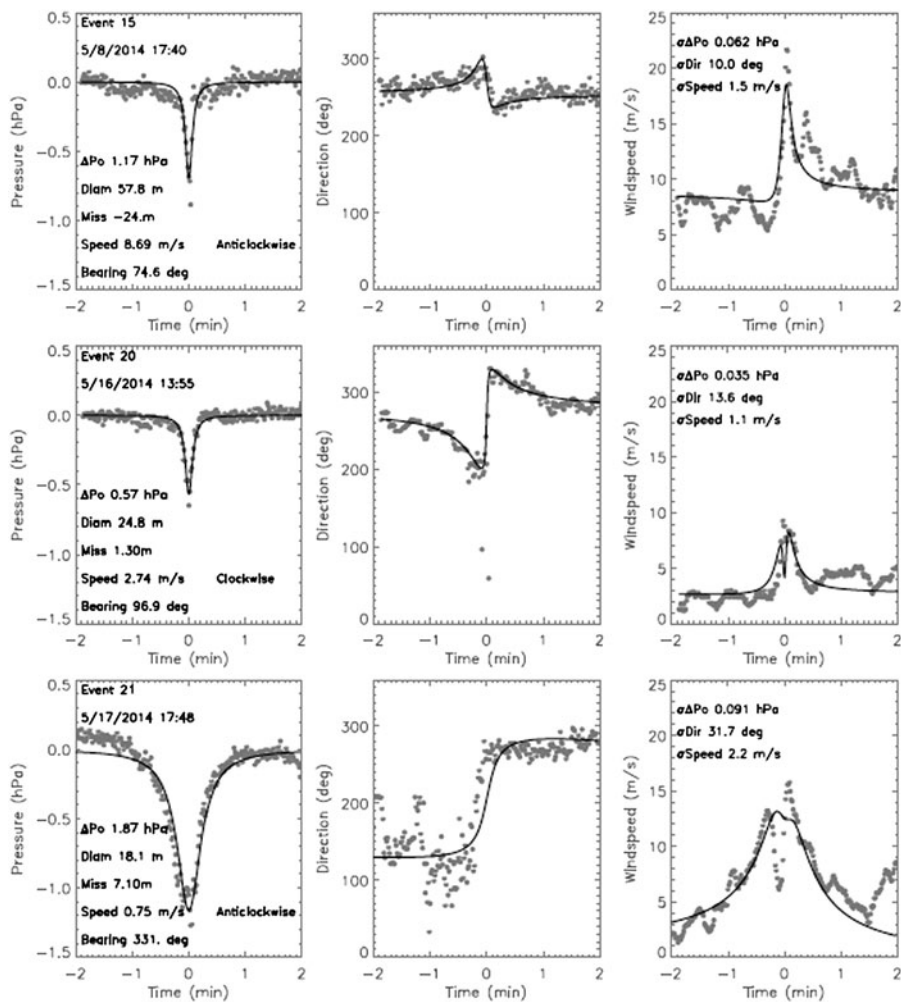
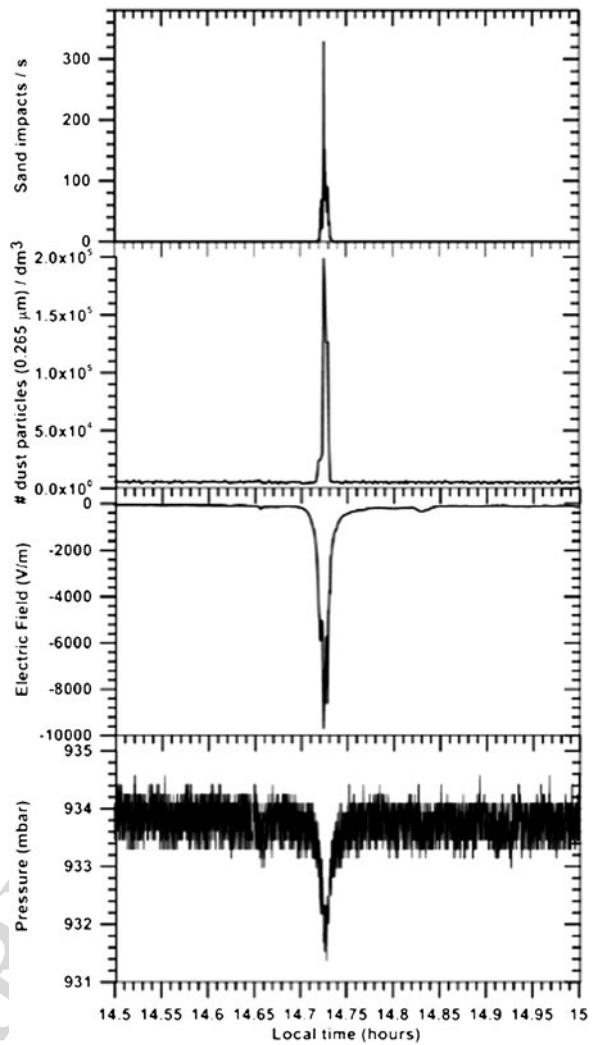


**Fig. 11** Three encounters with 1-Hz pressure, wind direction and speed (left to right) data (grey points) of dust devils at La Jornada (Lorenz 2016) with vortex model fits (black lines). The wind direction histories are particularly distinctive—speed histories tend to be somewhat noisy. It may be noted that the ‘eye’ of the vortex, where near-solid-body rotation within the wall results in very reduced windspeed at the center of the devil, clearly resolved in the lower-right plot (although not well captured by the model fit)

The 2014 West Sahara Campaign depicted in Esposito et al. (2016a, 2016b) has also been the opportunity to test the Micro-ARES electric field sensor of the DREAMS (Dust Characterisation, Risk Assessment, and Environment Analyser on the Martian Surface) science package for ExoMars 2016 (Bettanini et al. 2014). The instrument is based on the Relaxation Probe principle (Berthelier 2000, Molina-Cuberos et al. 2010) which requires a more complex post-processing than a classic field-mill sensor. One of the capabilities that had to be tested was the ability for the instrument to detect the electric field variations during the nearby passage of a dust devil, the passage being confirmed by the classical weather measurements. It appears that such events have been observed (Fig. 14) during the 4 days campaign and properly detected by the instrument. A more detailed study of the results will

**Fig. 12** An example of the electric field accompanying a dust devil as measured by Esposito et al. (2016a, 2016b) in the West Sahara desert: atmospheric electric field enhancement



show if the instrument is able to detect single particle collisions with the electrode, thus giving access to the particle electric charge during such events. A more detailed overview of the Micro-ARES and the results gathered during the 2014 West Sahara Campaign is presented in Harrison et al. (2016) in this issue.

**Seismic Signals** Pressure fluctuations in the atmosphere induce an elastic response in the ground that can be detected as a ground tilt by seismic stations installed on, or close to, the Earth's surface. This effect has been known since the 1970s (Sorrells 1971; Sorrells et al. 1971) and is one of the reasons that terrestrial seismic stations are typically installed deep underground in vaults.

The InSight lander mission, selected under the NASA Discovery programme and now scheduled for a May 2018 launch, will perform the first comprehensive surface-based geophysical investigation of Mars. The seismic instrument SEIS (Seismic Experiment for Internal Structures) is the critical instrument for delineating the deep interior structure of Mars

## Field Measurements of Terrestrial and Martian Dust Devils

**Fig. 13** Correlation between the abundance of lifted dust and the intensity of atmospheric electric field during dust storms (*red marks*) and dust devils (*blue marks*) and dust devils (*blue marks*)

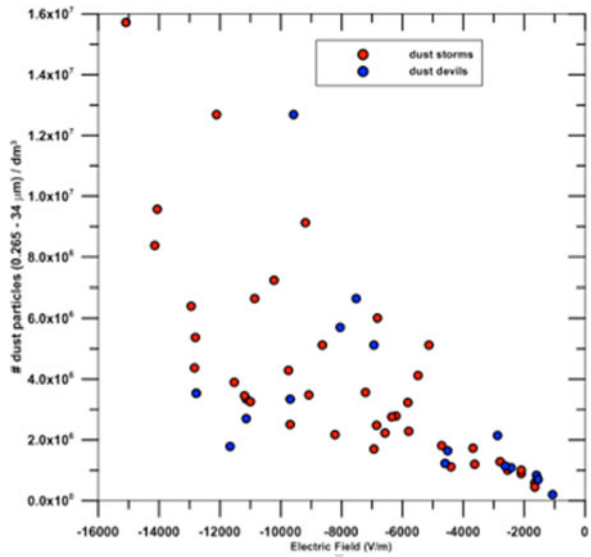
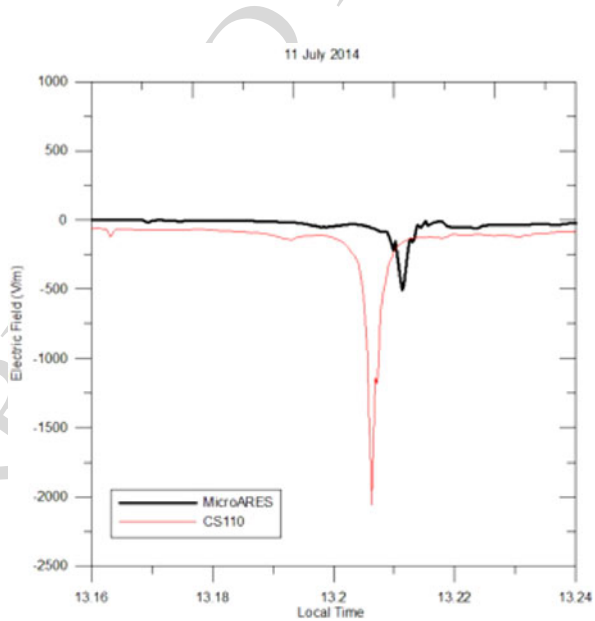


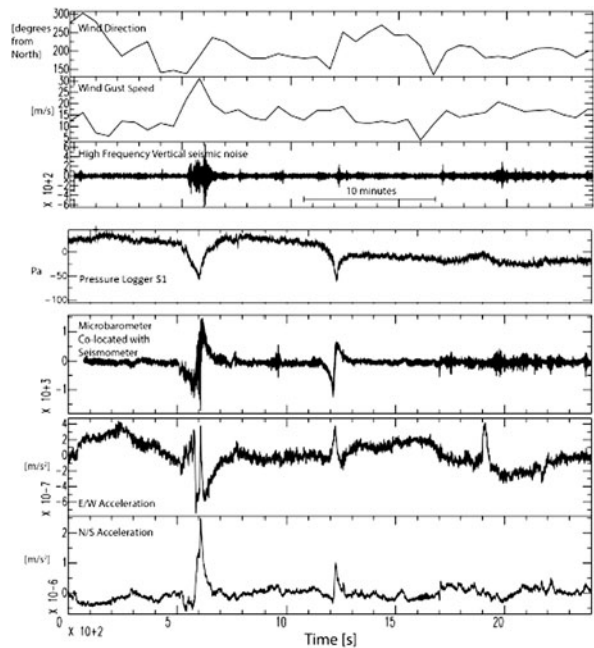
**Fig. 14** Comparison of Micro-ARES and Commercial Field-mill sensor DC measurements during a dust-devil event confirmed by pressure and wind parameters measurements. The amplitude and time differences are explained by the installation height (respectively 0.8 and 2 m) of the instruments and their distance (approx. 30 meters)



(Lognonné et al. 2012). SEIS will be deployed directly onto the surface of the planet and will, therefore, be sensitive to the atmospheric seismic signals. In fact, due to the lack of microseism-producing oceans, such atmospheric seismic signals are likely to be the dominating background seismic noise on Mars (Lognonné and Mosser 1993).

In preparation for the InSight mission, and to understand the effects of a surface deployment of a seismometer, representative field experiments were carried out in California close to the Goldstone Deep Space Communications Complex (Lorenz et al. 2015a). The experiment included a seismometer buried at very shallow depth, together with a suite of meteorological instruments. During this field campaign, ground tilt was measured by the

**Fig. 15** Two distinct seismic signals recorded during the passage of tow dust devils during mid-afternoon in late spring (2014) on a playa in the Mojave Desert, USA. The seismic measurements were accompanied by pressure and wind measurements; time was not precisely synchronized between the two sets of measurements; the meteorology measurements have been time shifted to coincide with the seismic signals. A third seismic signal (at  $\sim 19$  minutes) is not accompanied by a meteorologically detected dust devil. [After Lorenz et al. 2015b]



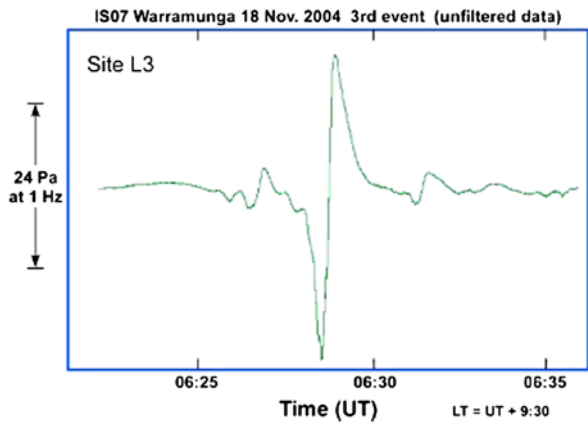
seismometer at the same time as vortex encounters were documented by an array of pressure loggers (Lorenz et al. 2015a). The negative load of a dust devil vortex pulls up the ground as it passes, causing the ground—and seismometer—to tilt away from the dust devil center. This first identification of the isolated seismic signature of a dust devil has shown that a seismometer appears to be capable of tracking close encounters with dust devils and, in addition, that seismometers may be more effective than in-situ meteorological instruments at detecting dust devils at long-range (Lorenz et al. 2015a).

Peak surface accelerations of  $1\text{--}2 \times 10^{-6} \text{ m}^2 \text{ s}^{-1}$  were measured during the passage of a dust devil presenting a measured pressure drop of 80 Pa (0.8 millibars) accompanied by a measured 2 % decrease in the short-circuit current of a solar cell mounted with a pressure logger located 30 meters from the seismometer (Fig. 15). The measured acceleration magnitudes and knowledge of the local surface material structure provided by a seismic survey enabled estimation of the dust devil's decreased surface mass loading/negative point load on an elastic half-space. The measured acceleration values and inferred vortex center miss distances imply a mass load of  $\sim 8000$  Newtons and tilt accelerations of  $7 \times 10^{-7} \text{ m s}^{-2}$  for a 5-meter diameter vortex with a central pressure deficit of 200 Pa passing 10 meters from the seismometer. A larger diameter (100 meter) dust devil also with a 200 Pa central pressure deficit could provide a total mass load of 300 metric tons and accelerations of  $10^{-6}\text{--}10^{-5} \text{ m s}^{-2}$  for miss distances of 50–200 meters, though the size of such a dust devil violates consideration of it as a point-source. The seismometer system employed by Lorenz et al. (2015a, 2015b, 2015c) included a microbarograph that coincident with the seismic signals registered the tell-tale infrasound 'heartbeat' dust devil signature identified by Lorenz and Christie (2015).

**Infrasound and Acoustic Measurements** It was noted by Lorenz (2012a, 2012b) that while meteorological stations tend to record data at only 15-minute intervals, continuous pressure measurements, made with sufficient sensitivity and sample rate to detect dust devil

## Field Measurements of Terrestrial and Martian Dust Devils

**Fig. 16** Microbarograph measurement of a dust devil pressure signature, showing the up-down heartbeat signature of the vortex. Two additional smaller amplitude subsidiary events are present  $\sim 1$  minute before and 2 minutes after the primary event. [After Lorenz and Christie 2015]



vortices are made for other applications, notably for monitoring compliance with international treaties on nuclear testing. Some of these stations, operated by the Comprehensive Test Ban Treaty Organization (CTBTO) are located in desert areas, and dust devil vortex signatures at a CTBTO station in Australia are reported by Lorenz and Christie (2015). Since atmospheric effects are a major perturbation to seismic signals, many seismic stations (such as those in the USARRAY) now also record pressure and other meteorological parameters. Data-mining of such records may be a fruitful avenue of research. A subtlety to be noted is that microbarographs used for infrasound studies (and those e.g. at CTBTO stations) are high-pass-filtered pressure records, such that the principal component in the signal is the derivative of the pressure signal. Thus the typical dip seen in pressure time series in fact appears as a down-up-down 'heartbeat' signature (Fig. 16).

Lorenz and Christie (2015) investigated dust devil pressure signatures within microbarograph measurements obtained as part of CTBT monitoring from a station located in Australia. The high pass filtered signal of a dust devil pressure measurement appears as a 'heartbeat' signal that resembles the temporal derivative of measured pressure provide by a pressure sensor with a sampling of  $\sim 1$  Hz. This heartbeat signal exhibits declining signal magnitude as the pressure minimum is approached and an abrupt transition in the sign of the signal to a maximum magnitude that subsequently declines in concert with the measured pressure increase as the dust devil's influence wanes. Contemporaneous microbarograph and pressure sensor measurements verify the dust devil production of the microbarograph's heartbeat signal. While this is not a direct measure of the infrasound generation produced by a dust devil, it is a distinct signal from which dust devil occurrence can be derived.

Edmonds (2014) attempted to detect the infrasound emission that a dust devil, or that interacting dust devil vortices, might produce. Theory (Powell 1964; Howe 2003) indicates that two vortices 'orbiting' around each other are capable of generating infrasound emission, as is a single non-circular vortex (Howe 2003). Williams (2001) addressed the attenuation of acoustic signals within Mars' tenuous atmosphere and concluded that infrasound frequencies ( $< 20$  Hz) at which dust devils are effective emitters (Bedard 2005) experience smaller dissipation than do higher audible frequencies. That work was motivated by the inclusion on the ill-fated 1999 US/NASA Mars Polar Lander of a microphone intended to listen for martian sounds. Edmonds' (2014) work was motivated by the inclusion on the NASA InSight lander of a high-frequency pressure sensor (Banfield 2014). Edmonds (2014) conducted a field exercise in the desert of southern New Mexico, USA in Spring 2014 attempting to detect the infrasound and audible frequency emission from dust devils. Using

1351 a microphone/recording acoustic system and a microbarograph, three dust devils recorded  
1352 from distances of a few to 10's of meters coincided with measured audible ( $> 20$  Hz) sig-  
1353 nals. The recordings indicate amplitude 'ridges' within distinct acoustic frequency ranges,  
1354 distinct from sounds attributed to wind-induced movement of vegetation objects (vegetation,  
1355 sand, etc.). However, no infrasound detection was identified.  
1356

### 1357 **3.2 Mars Surface Obtained Meteorological Measurements of Dust Devils**

1358

1359 While there has been until recently a general dearth of seasonal or longer temporal cov-  
1360 erage of terrestrial dust devil in situ measurements arising from limited duration measure-  
1361 ment campaigns, but a plethora of measured dust devil parameters/characteristics from these  
1362 same studies, in situ measurement of martian dust devils has suffered from opposite condi-  
1363 tions. Martian lander and rover missions have provided durations extending from 83 sols  
1364 (Pathfinder) to multiple martian years (Viking Lander 1 spanned more than 3 Mars years,  
1365 Spirit Rover 3 Mars years, Opportunity Rover 6+ Mars years and continuing, and MSL  
1366 almost two Mars years and counting). However, some missions have suffered from me-  
1367 teorological instrument failures (Viking Lander 1, MSL) or calibration issues (Pathfinder)  
1368 while others did not carry any direct meteorological instruments at all (Opportunity, Spirit).  
1369 The robotic vehicles that did carry meteorological instrumentation generally have provided  
1370 high frequency, one to a few Hz, sampling sufficient to characterize dust devil signatures  
1371 but did not do so continuously, except for the Phoenix Lander. It is from the measurements  
1372 provided by the five meteorology-instrumented vehicles (Viking Landers 1 & 2, Pathfinder,  
1373 Phoenix, MSL) that our current thermodynamic understanding of martian dust devils has  
1374 been obtained.  
1375

1376 A compilation of measured characteristics is provided in Table 2.  
1377

#### 1378 *3.2.1 Viking Landers*

1379

1380 The two US/NASA Viking Lander spacecraft which arrived at Mars in 1976 provided the  
1381 first opportunity for in situ sensing of the meteorological signatures of passing martian dust  
1382 devils. Viking Lander 1's landing location was 23 N, 48 W, while Viking Lander 2's was  
1383 48 N, 226 W.

1384 As previously described, a characteristic transient drop in atmospheric pressure is de-  
1385 tected when a convective vortex passes over/near a deployed pressure sensor, as has been  
1386 amply demonstrated for terrestrial dust devils. The digital quantization of the long lived  
1387 Viking lander pressure sensors was 8.8 Pa (Hess et al. 1977; Tillman et al. 1993), which  
1388 subsequent missions (Murphy and Nelli 2002; Ellehoj et al. 2010) indicated was too large  
1389 to unambiguously detect a martian dust devil pressure signature of several Pascals or less  
1390 magnitude. Additionally, the Viking Lander pressure measuring strategy was not generally  
1391 focused upon detection of short duration events but rather upon characterization of diurnal  
1392 and seasonal variations. A typical time interval between pressure measurements was 17 min-  
1393 utes (Ryan and Lucich 1983). Pressure sampling did include some brief time periods early  
1394 in the mission during which measurements were obtained at a rate of  $\sim 1$  per second, but  
1395 much more often sampling rates were once each 16 or 32 seconds extending to once per 65  
1396 to 105 minutes. There is no publication that addresses assessment of the complete Viking  
1397 lander pressure record for identification of dust devil/convective vortex signatures. The VL1  
1398 pressure record spans from  $L_s$  97.1 (MY 12) through  $L_s$  226.7 (MY 15), while VL2 spans  
1399  $L_s$  117 (MY12) through  $L_s$  57.1 (MY 14).  
1400

1401 While Viking Lander pressure measurements were not amenable to dust devil studies,  
1402 Viking's measured winds were. Ryan and Lucich (1983) investigated wind vector measure-  
1403 ments provided by Viking Meteorology Instrument System (VMIS) at both landers, with  
1404 measurement sampling intervals ranging from 2–112 seconds. Vortices were identified by  
1405 temporal rotation of the measured wind direction accompanied by a concurrent wind speed  
1406 variation illustrative of an imbedded Rankine-type vortex, and a concurrent temperature  
1407 maximum. A total of 118 vortices were identified during the mission's first year, 40 vortices  
1408 at VL1 spanning summer through winter and 78 at VL2 spanning summer through spring.  
1409 The greatest likelihood of vortex detection occurred almost equally ( $\sim 65\%$  of the sols  
1410 investigated) at VL1 during summer and VL2 during spring.

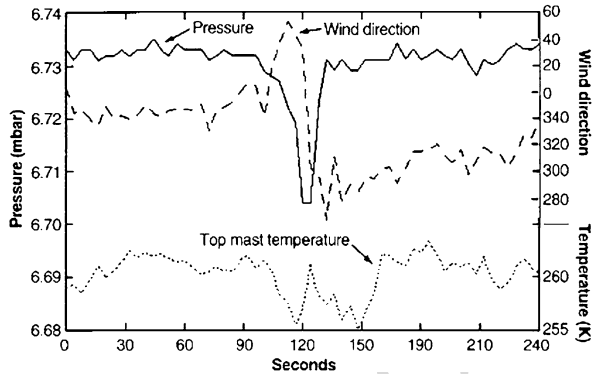
1411 Identified vortex disturbance influence persisted for several to  $\sim 10$  minutes, with the  
1412 most pronounced vortex effects present for tens of seconds to several minutes. Inferred vor-  
1413 tex core diameters, the distance from vortex center at which tangential wind speed max-  
1414 imized, were generally tens to several hundreds of meters, with radii of disturbance ef-  
1415 fects extending out ten times the core radius. Several inferred core diameters extended to  
1416  $\sim 500$ – $1000$  meters, implying radii of vortex influence extending to  $\sim 5$ – $10$  km. Inferred  
1417 vortex rotation was equally divided between cyclonic ('counter-clockwise') and anticyclonic  
1418 ('clockwise'), consistent with terrestrial experience (Sinclair 1973) and suggestive that the  
1419 vorticity is generated locally at small scales. Several of the vortices at both Viking lander  
1420 sites were sufficiently intense to generate winds ( $> 35 \text{ m s}^{-1}$ ) deemed capable of lifting  
1421 surface dust (Greeley and Iversen 1985). There were no concurrent imaging observations  
1422 invoked to address the presence or lack of dust in the detected vortices.

1423 It is unclear how unambiguous VL1 wind directions employed in this investigation were  
1424 derived subsequent to sol 45 and the failure of the wind direction quadrant sensor (Murphy  
1425 et al. 1990). VL2's wind instrument did not suffer from such a failure.

1426 Ringrose et al. (2003) readdressed the dust devil/convective vortex signatures present in  
1427 Viking Lander 2 wind measurements. Using a phase picker detection technique compar-  
1428 ing a running mean value to a threshold value (also used terrestrially in Hecht et al. 2001),  
1429 instances where a short term average wind speed or wind direction varied by more than  
1430  $6 \text{ m s}^{-1}$  or 40 degrees azimuth, respectively, from longer term averages were flagged as pos-  
1431 sible vortex signatures. For verified vortex signatures, minimum distance from the vortex  
1432 center and vortex diameter were derived from a Rankine vortex fit to the measured wind.  
1433 Applying this technique to VL2's first 60 sols resulted in 38 identified vortex occurrences,  
1434 nine of which suffered from lander interference which makes them suspect. Maximum mea-  
1435 sured wind speeds were  $12$ – $15 \text{ m s}^{-1}$  and maximum wind vector rotation was 300 degrees.  
1436 Inferred vortex core diameters arising from the Rankine vortex fits ranged from a few  $10$ 's to  
1437 a few hundred meters. Detected vortex durations ranged from  $60$ – $1080$  seconds. Maximum  
1438 inferred vortex core diameter tangential wind speeds were  $\sim 100 \text{ m s}^{-1}$  for two events. These  
1439 two events coincided with the largest inferred 'miss distance from core center' ( $\sim 1700 \text{ m}$ )  
1440 and largest vortex core diameters ( $> 350 \text{ m}$ ), while maximum inferred speeds for smaller  
1441 ( $< 250 \text{ m}$ ) miss distances and smaller core diameters ( $< 100 \text{ m}$ ) ranged from  $3$  to  $70 \text{ m s}^{-1}$ .  
1442 Daytime hour-of-occurrence of detected vortices exhibited late morning and early afternoon  
1443 maxima. A secondary minimum was also evident at 0930 local time. There was no descrip-  
1444 tion of the completeness of coverage of measurements during the 30-minute time intervals  
1445 into which the vortex occurrences were binned for this time-of-sol evaluation, so the time-  
1446 of-sol distribution might not be representative of conditions.

1447 Measured atmospheric temperature increases of several degrees Centigrade accompanied  
1448 some, but not all, of the wind-detected vortices identified by both Ryan and Lucich (1983)  
1449 and Ringrose et al. (2003).

**Fig. 17** Mars Pathfinder ASI/MET measured Time series of 0.25 Hz pressure, temperature, and wind direction during a 4-minute time period during the early afternoon of Sol 25 of the mission. After Schofield et al. (1997)



The Viking Landers did provide for the first time in situ evidence of martian convective vortices, in the form of wind vector temporal variation consistent with the passage of a vortex. Vortex occurrences were frequent, with at least one-half of the mission sols investigated possessing a detected vortex occurrence. This detection rate is certainly a lower limit since VMIS was not in continuous operation during any of the sols investigated.

### 3.2.2 Mars Pathfinder

From its northern subtropical landing location, Pathfinder provided pressure measurements that spanned the mission's 83 late summer-early autumn sols. Pathfinder's deflecting diaphragm, variable reluctance pressure sensor (Seiff et al. 1997) provided 14-bit,  $\sim 0.25$  Pa resolution in its 600–1000 Pa surface operating mode. While Pathfinder's Atmospheric Structure Investigation/Meteorology (ASI/MET) system (pressure, temperature, wind) generally provided greater temporal sampling resolution (0.25 to 2 Hz) than did the Viking Lander's, ASI/MET like Viking VMIS was not continuously operated. During the mission's first  $\sim 30$  sols, 3-minute, 0.25 Hz measuring sessions initiated at the start of most LTST hours were augmented by 15-minute and 60-minute continuous measurement sessions at 1 Hz sampling cadence. On five occasions during the mission, the first starting at 0600 LTST of Sol 25, the ASI/MET system was continuously operated for a complete sol at a sampling rate of 0.25 Hz. These 'Presidential MET' sessions were initiated on Sols 25, 32, 38, 55, and 68. Subsequent to Sol 30, the ASI/MET system was operated during daylight hours only,  $\sim 0900$ – $1600$  LTST, except during the Presidential MET sessions.

Schofield et al. (1997) presented the first in situ contemporaneous measurement of pressure, wind and temperature within a martian dust devil/convective vortex, from measurements obtained during early afternoon, 1353 LST, during the Sol 25-initiated Presidential MET session (Fig. 17). The quantified vortex pressure drop magnitude was  $\sim 2.5$  Pa. Subsequently, Murphy and Nelli (2002) assessed the entire Pathfinder pressure data archive and identified the occurrence of 79 vortices,  $\sim 1$  per sol, with pressure drop magnitudes equal to or exceeding 0.5 Pa. Vortex identification was based upon a pressure drop magnitude determined from the difference between a 3rd order polynomial fit to measured pressures during a 15-minute interval and the unaltered pressure measurements. The maximum pressure drop magnitude identified was 4.8 Pa at 1132 LST on Sol 34. The LST time of detection of the 79 vortices spanned 0930–1700.

The discontinuous temporal coverage provided by ASI/MET indicated that the true number of detectable vortices would exceed 79. Normalizing the number of vortices detected

1501 throughout the mission during each 15-minute LST time window by the percentage of time  
1502 the ASI/MET system was operating during that 15-minute window resulted in an estimate  
1503 of 210 detectable vortices occurring during the 83 sol mission, equating to  $\sim 2.5$  vortices  
1504 per sol. This 2.5 per sol estimate is less than the  $\sim 4$  vortices per sol detected during the five  
1505 Presidential MET sols of almost continuous pressure sensor operation (Murphy and Nelli  
1506 2002).

1507 Ferri et al. (2003) determined the duration of 19 of the larger magnitude ( $> 1$  Pa) pressure  
1508 signature events identified by Murphy and Nelli (2002). Durations ranged from 14–51 sec-  
1509 onds, with a mean value of 28 seconds and median value of 25 seconds.

1510 Both the directly detected and normalized inferred Pathfinder vortex occurrences exhib-  
1511 ited a maximum hourly occurrence during very early afternoon (Fig. 18). Vortex activity  
1512 after the early afternoon peak declined more gradually than through the afternoon than its  
1513 increase during the morning.

1514 Applying Metzger et al.'s (1999) visible plume dust mass load estimates and the fre-  
1515 quency of occurrence derived from the Pathfinder pressure measurements, Murphy and Nelli  
1516 (2002) estimated that local dust devil activity could provide dust to the atmosphere at the  
1517 rate of an optical depth of 0.01 per sol over a 1.5 km diameter area centered upon the lander.  
1518 This estimate is approximately equal to the opacity decay rate measured during the decline  
1519 of the second global scale martian dust storm during 1977 (Pollack et al. 1979).

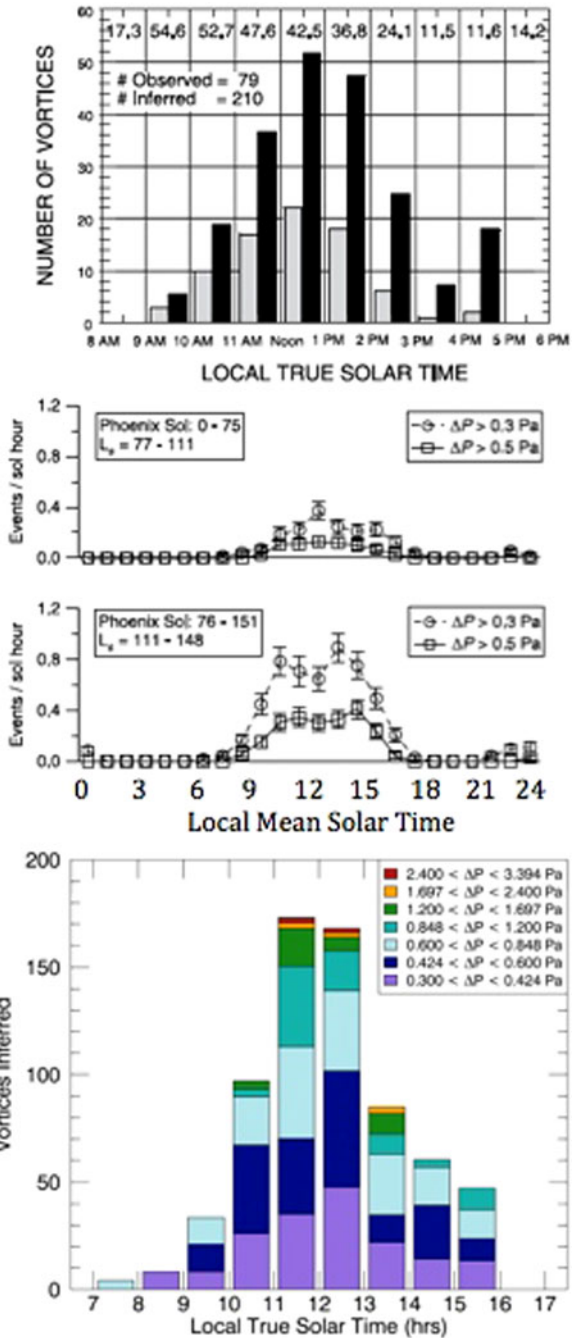
1520 Pathfinder's ASI/MET system included a wind sensor (Seiff et al. 1997). Additionally,  
1521 a 'wind sock' was mounted on the ASI/MET mast with IMP-provided images enabling wind  
1522 vector derivation from observed windsock orientation (Sullivan et al. 2000). The ASI/MET  
1523 wind sensor was a thermal/mechanical instrument using the measured overheat of resistively  
1524 heated sensor elements (wires) from which wind speed and direction were intended to be  
1525 derived. The sensor consisted of a vertically oriented 2.7 cm diameter, 3 cm tall solid exte-  
1526 rior cylinder around which were arrayed six 'segments' of azimuthally confined vertically  
1527 aligned 8-wire length windings. A pulsed 20 milliamp current provided unheated segment  
1528 wire temperature from measured voltage drops across each segment. When the sensor was  
1529 operated in a continuous 52 milliamp high current mode the segment wire temperatures were  
1530 resistively heated. Segments positioned in the upwind direction experienced ventilative cool-  
1531 ing, with overheat magnitudes and their azimuthal structure providing the signal indicative  
1532 of the wind vector. The sensor was not designed with its own reference temperature against  
1533 which segment temperature could be assessed for 'overheat' magnitude. It was anticipated  
1534 that thermocouples mounted on the ASI/MET would provide the reference temperature.  
1535 However, large magnitude 'turbulent' temperature variations ( $\sim 10$ – $15$  K; Schofield et al.  
1536 1997) inhibited unambiguous determination of a reference temperature for wind sensor seg-  
1537 ment overheat determination purposes.

1538 The wind sensor was generally operated for  $\sim 12$  seconds of low-current pulsed mode  
1539 to establish unheated segment temperatures, after which continuous high current was im-  
1540 posed for  $\sim 150$  seconds. It would be during these 150 second intervals that wind speed and  
1541 direction could be quantified.

1542 Despite these unresolved operational/calibration issues for the Pathfinder wind sensor,  
1543 the sensor did provide signals that were qualitatively correlated to dust devil occurrences  
1544 identified in Pathfinder's pressure measurements (Murphy and Nelli 2002; Schofield et al.  
1545 1997). Wind sensor signals did suggest substantial and abrupt changes in wind direction and  
1546 speed in conjunction with measured dust devil pressure signatures (see, for instance, Fig. 8  
1547 in Schofield et al. 1997), however no systematic study of vortex winds has been published.

1548 In addition to the ASI/MET's thermal wind sensor, Pathfinder also included three me-  
1549 chanical 'wind socks' mounted at three heights along the ASI/MET mast (Sullivan et al.

**Fig. 18** Martian dust devil occurrence frequency versus time-of-sol from pressure signatures from Mars Pathfinder (top; Murphy and Nelli 2002), Mars Phoenix (middle; Ellehoj et al. 2010) and Mars Science Lab (bottom; Steakley and Murphy 2016)



2000). IMP provided images of the solid, metallic, inverted-cone shaped socks and their tilt orientation from which wind speed and direction were derived using pre-flight calibration information. Twelve image sequences obtained over a time period of ~ 100 seconds several

1601 times per sol provided the dataset from which wind vector derivation was attempted. Data  
1602 from only four of the sampled 42 sols provided imaging indicative of minimum wind speed  
1603 (few meters per second) necessary to overcome windsock inertia and induce detectable  
1604 windsock deflection (Sullivan et al. 2000). Thus, Pathfinder's windsock experiment did not  
1605 aid in advancing understanding of the dynamic components of martian dust devils.

1606 Schofield et al. (1997) noted that one pressure-indicated vortex passage detected by MPF  
1607 was accompanied by a transient drop in output from the lander's solar panels, suggesting  
1608 that the vortex was dust-laden and the dust column created at least a partial shadow that  
1609 crossed the lander. This observation underscores the utility of making available engineering  
1610 data such as solar array current data from lander missions—in effect the arrays serve as a  
1611 'free' instrument.

### 1612 1613 3.2.3 Mars Exploration Rovers (*Spirit and Opportunity*) 1614

1615 Neither Spirit nor Opportunity were outfitted with meteorological measuring instrumenta-  
1616 tion. The MERs' mini-TES instrument was used to diagnose the vertical atmospheric struc-  
1617 ture within the bottom few hundred meters to 1–2 km (Smith et al. 2004). While those  
1618 measurements illustrated the superadiabatic conditions present during mid-sol, there was no  
1619 identification of such a measurement probing a dust devil.

1620 It had been noted during the MPF mission that a calibrated solar cell on the Sojourner  
1621 rover recorded a progressive decline in cell current of  $\sim 0.25\%$  per day (Landis and Jenkins  
1622 2000), due to the accumulation of airfall dust on the cell. This obscuration set expectations of  
1623 operational lifetime of solar-powered landers and rovers on Mars (e.g. the Mars Exploration  
1624 Rovers Spirit and Opportunity had a nominal mission duration of 90 days).

1625 In practice, it was observed that while the MER solar power per day declined due to  
1626 dust accumulation, sudden reversals of the decline were seen, and camera images of the  
1627 arrays showed that dust had been removed. While dust devils were suspected, the like-  
1628 likelihood remains that straight-line gusts may have been responsible. However, Lorenz and  
1629 Reiss (2015) showed that not only did the seasonal onset of dust-clearing events coincide  
1630 with the appearance of dust devils (Greeley et al. 2006; 2010), but also the rate at which  
1631 dust-clearings occurred was coincident with the rate of vortex encounters seen in pressure  
1632 drops by Phoenix and Pathfinder, extrapolated to a dust lifting threshold of a few Pa.

### 1633 1634 3.2.4 Mars Phoenix Lander 1635

1636 The US/NASA Phoenix lander meteorologically detected, at its northern arctic latitude land-  
1637 ing site, dust devil/convective vortex signatures that complement its SSI imaging dust devil  
1638 detections (Sect. 2b). Phoenix was equipped with a meteorological package (MET), includ-  
1639 ing pressure, air temperature and wind sensors and a Light Detection And Ranging (LI-  
1640 DAR) instrument for measuring dust and ice particles in the atmosphere (Taylor et al. 2008;  
1641 Whiteway et al. 2008). The pressure sensor was based on Barocap<sup>®</sup> silicon diaphragm sen-  
1642 sor heads manufactured by Vaisala Inc. and had a very high resolution of 0.1 Pa (Taylor  
1643 et al. 2010), limited by the noise level. In contrast to the Vikings, Pathfinder and MSL,  
1644 Phoenix logged atmospheric pressure and air temperature almost continuously, with an in-  
1645 variant sampling rate (0.5 Hz) (Taylor et al. 2010; Davy et al. 2010). The mission spanned  
1646 151 sols, almost twice the duration of the Pathfinder mission, extending from early spring  
1647 through mid northern hemisphere summer ( $L_s$  77° to  $L_s$  148°). The continuous Phoenix  
1648 pressure record enabled the detection of a greater number of convective vortices than had  
1649 Pathfinder.

1651 Ellehoj et al. (2010) surveyed the entirety of pressure measurements provide by Phoenix  
1652 and identified 502 ( $\sim 3.3$  per sol) transient pressure drops similar to the vortex signatures  
1653 that Murphy and Nelli (2002) had detected in the Pathfinder data. The magnitudes of these  
1654 Phoenix pressure drops ranged from 0.3 Pa (an imposed lower limit) to 3.6 Pa, with 197  
1655 occurrences possessing a magnitude greater than the 0.5 Pa detection threshold used by  
1656 Murphy and Nelli (2002). Vortex identification was based on the search for 20 s long time  
1657 intervals that fulfilled the following two criteria: 1) mean pressure more than 0.1 Pa lower  
1658 than mean of the previous and next 20 s intervals, and 2) minimum pressure more than 0.3 Pa  
1659 lower than mean of the previous and next 20 s intervals.

1660 The Full Width at Half Maximum (FWHM) durations of events with magnitude  $> 0.5$  Pa  
1661 ranged from less than 1 s to circa 35 s, the mean being circa 9 s (Table 1 in Ellehoj et al.  
1662 2010). [Note that there is a typographical error in the caption of Fig. 7 in the Ellehoj et al.  
1663 (2010); the shown quantity is actually full duration, i.e.  $2 \times$  FWHM (H. P. Gunnlaugsson,  
1664 Aarhus University, personal communication, 2015)]. It is unclear if these durations are com-  
1665 parable to the durations reported by Ferri et al. (2003) for the Pathfinder pressure drops, as  
1666 Ferri et al. (2003) did not explain how their durations are defined.

1667 Most transient pressure drop events identified in the Phoenix data occurred between  
1668 06:00 and 18:00 Local Mean Solar Time (LMST). However, unlike Pathfinder, Phoenix also  
1669 detected also 29 events between 21:00 and 01:00 LMST (mostly with the Sun low in the  
1670 arctic sky), interpreted as being caused by turbulence induced by air passing over Heimdal  
1671 crater, the only major topographic feature in the vicinity of the lander (Ellehoj et al. 2010).  
1672 The general shape of the diurnal distribution of vortex activity resembled that detected by  
1673 Pathfinder, but at the Phoenix site the vortex activity stayed high until circa 15:00 in the  
1674 afternoon while at the Pathfinder sites the activity started to fall already at circa 13:00.

1675 Phoenix operated long enough to detect some seasonal variation in vortex activity. The  
1676 number of identified transient pressure drops generally increased around Phoenix sol 75  
1677 ( $L_s = 111$ , about 40 sols after summer solstice and 15 sols before the Sun set for the first  
1678 time) and the proportion of events with large pressure drops became higher at the same time  
1679 (Ellehoj et al. 2010). Before this, an average of 0.6 events with magnitude  $> 0.5$  Pa were  
1680 observed per sol, but after this 2.0 events per sol, a number comparable to the estimated  
1681 number of vortices that passed by Pathfinder per sol during the same season. Phoenix also  
1682 detected more frequent vortex activity coinciding with passing cold fronts associated to  
1683 low-pressure baroclinic systems. The clearest example of this was Phoenix sol 95, when  
1684 36 pressure drops larger than 0.3 Pa were identified in contrast to 6 and 7 vortices on the  
1685 preceding and following sols, respectively. A concurrent cloud feature suggestive of a cold  
1686 front was seen to cross the Phoenix landing site in images taken by the Mars Color Imager  
1687 (MARCI) onboard the Mars Reconnaissance Orbiter on that sol (Ellehoj et al. 2010).

1688 The payload on the Mars Phoenix lander included a mechanical wind sensor, the so-  
1689 called Telltale (Gunnlaugsson et al. 2008; Holstein-Rathlou et al. 2010), consisting of a  
1690 lightweight cylindrical mass dangling on a thread attached to a crossbar at the top of the me-  
1691 teorological mast. The Telltale was designed to be deflected by wind and the deflection was  
1692 observed by imaging the Telltale with the SSI. SSI did not monitor the Telltale continuously.  
1693 Imaging sequences were implemented during only a limited number of hours per sol, and  
1694 during these sequences readings were acquired with time intervals longer than 50 seconds  
1695 (Holstein-Rathlou et al. 2010).

1696 Telltale imaging on nine occasions occurred within 10 seconds of a pressure minimum  
1697 associated to a passing vortex (Ellehoj et al. 2010). In these events the wind vector was ob-  
1698 served to differ by 1.4 to 9.3  $\text{m s}^{-1}$  from background wind speeds, magnitudes greater than  
1699 typical changes between consecutive Telltale images. This observed magnitude range of the  
1700

wind vector perturbations is in agreement with the range of the observed pressure drops assuming cyclostrophic balance (Ellehoj et al. 2010). Even the strongest vortex-related wind perturbation detected from Telltale measurements, however, is below any estimate of the dust lifting threshold on Mars (Neakrase and Greeley 2010), which is not surprising considering that the derived wind speeds are ‘snapshots of the wind in random points inside a vortex, not maximum wind speeds, and the great majority of the vortices detected by pressure measurements on Mars are actually too weak to lift dust (Moores et al. 2015; Kahanpää et al. 2016; Steakley and Murphy 2016).

### 3.2.5 MSL

MSL’s Rover Environmental Monitoring Station (REMS) includes sensors for pressure, air and ground temperature, wind speed and direction, humidity and UV radiation measurements (Gómez-Elvira et al. 2012). REMS executes five-minute 1 Hz data acquisition sessions at the start of each LMST hour, with 15 minute and one hour 1 Hz “extended measurement blocks” implemented at variable times of the sol (Gómez-Elvira et al. 2014). The REMS pressure sensor is, as was MET Phoenix, comprised of Vaisala Barocap® silicon diaphragm sensor heads. REMS’ pressure sensor noise is slightly higher (0.2 Pa peak-to-peak) as a result of the faster sampling rate and thus shorter integration time (Harri et al. 2014).

Two major studies have characterized the meteorological signatures of convective vortices identified in the MSL/REMS data (Kahanpää et al. 2016; Steakley and Murphy 2016), identifying dust devils from their temporary pressure declines using slightly different detection criteria. The Kahanpää et al. (2016) criteria are more consistent with the Phoenix dust devil detections (Ellehoj et al. 2010) while the Steakley and Murphy (2016) criteria are more consistent with the Pathfinder dust devil detections (Murphy and Nelli 2002). Despite the different identification criteria both studies come to similar conclusions about vortex activity at Gale Crater.

Few dust devils were anticipated within Gale Crater based upon a lack of observed dust devil tracks and a suggestion of a suppressed atmospheric boundary layer depth (Tyler and Barnes 2013; Haberle et al. 2014). However, approximately 250 pressure vortex signatures were identified during the first Martian year of the mission: Kahanpää et al. (2016) report 252 transient pressure drops with magnitude exceeding 0.5 Pa during the first 681 sols of the mission, and Steakley and Murphy (2016) report 245 pressure drops with magnitude exceeding 0.3 Pa during the first 707 sols of the mission. The largest reported pressure drop, 2.97 Pa and 2.86 Pa by Kahanpää et al. (2016) and Steakley and Murphy (2016), respectively, was detected on MSL sol 403 at 13:02 Local Mean Solar Time (LMST). Steakley and Murphy’s (2016) identification of fewer vortices than Kahanpää et al. (2016) despite their lower detection threshold and a 5 % longer study time is partly explained by their criterion that a pressure drop must have a magnitude clearly above background noise. This criterion probably deselects many pressure drops with magnitudes below 0.5 Pa. Also, some larger pressure drops reported by Kahanpää et al. are apparently deselected when local turbulence raises the noise level of the pressure signal. Moreover, Kahanpää et al. (2016) are less strict with the criterion that a pressure drop must have a “dust devil like” shape and they report many pressure events with several minima or otherwise irregular shape.

The Full Width at Half Maximum (FWHM) durations of the pressure drops reported by Kahanpää et al. (2016) follow a distribution almost identical to that reported by Ellehoj et al. (2010) for the Phoenix data, ranging from less than 1 s to circa 54 s, the mean being circa 9 s. Steakley and Murphy’s (2016) FWHM durations range from 1–20 seconds with a median value of 5.3 seconds.

1751 The time-of-sol distribution of MSL's daytime transient pressure drops resembles that  
1752 detected by Pathfinder and Phoenix, ranging from around 9:00 to 16:00 Local True Solar  
1753 Time (LTST) with maximum occurrence around noon (Kahanpää et al. 2016; Steakley and  
1754 Murphy 2016) (Fig. 18). Several night-time pressure 'wiggles' were also identified (Kahan-  
1755 pää et al. 2016). These night-time events exhibit wave-like fluctuations rather than isolated  
1756 pressure drops and are interpreted as the result of gravity waves initiated by topographic  
1757 winds (Haberle et al. 2014).

1758 The extended duration of REMS operation provides the first opportunity to assess sea-  
1759 sonal vortex occurrence from measured martian pressures. Kahanpää et al. (2016) estimated  
1760 the mean number of vortices per sol causing pressure drops larger than 0.5 Pa separately  
1761 for 8 "seasons" during MSL's first martian year. These estimates ranged from 0.5 per sol  
1762 ( $L_s$  s 67.5–112.5) to 1.8 per sol ( $L_s$  202.5–247.5). Steakley and Murphy (2016) find a  
1763 spring ( $L_s$  180–270) occurrence maximum of 1.5 per sol that is twice the minimum occur-  
1764 rence rate ( $L_s$  90–180). This continuous vortex occurrence through the year is in contrast  
1765 to the visual MER Spirit imaging observations of detected dust devils only during the "dust  
1766 devil season" (Greeley et al. 2010, referred in Sect. 2b), but is in rough accordance with the  
1767 vortex observations performed using the Viking wind data (Ryan and Lucich 1983).

1768 During MSL's first 681 sols there was only one case when more than 3 pressure drops  
1769 larger than 0.5 Pa were detected within the same LMST hour (Kahanpää et al. 2016). This  
1770 exception occurred on sol 664 when 16 pressure drops were identified by Kahanpää et al.  
1771 (2016) between 11:00 and 12:00 LMST. Steakley and Murphy (2016) also identified sol 664  
1772 as experiencing the greatest number, four, of verified vortices. This "sol 664 vortex burst"  
1773 resembles the peaks in vortex activity detected by Phoenix coincident with a passing dust  
1774 storm front seen in MARCI images.

1775 REMS includes a hot-film anemometer (Domínguez et al. 2008; Gómez-Elvira et al.  
1776 2012) designed to distinguish the 3-dimensional wind field. The sensor is mounted on  
1777 two horizontally aligned booms attached to MSL's Remote Sensing Mast (RSM) which  
1778 are separated by 120 degrees in azimuth. On each boom there are three identical hot-film  
1779 anemometer boards sensing wind speed in different directions. Unfortunately, three of the  
1780 altogether six boards were damaged during MSL's landing (Gómez-Elvira et al. 2014), initi-  
1781 ating an ongoing re-calibration effort. To date only 2-dimensional wind measurements have  
1782 been retrieved (Sara Navarro, Centro de Astrobiología/CSIC-INTA, personal communica-  
1783 tion, 2015). The compromised wind sensor raw data do qualitatively reveal wind variations  
1784 concurrent with the transient vortex pressure drops (Kahanpää et al. 2016), with 87 % of  
1785 the pressure drops being accompanied by wind sensor events. Magnitudes of these wind  
1786 perturbations could not be determined.

1787 Available quantified REMS wind measurements consist of derived 5-minute median val-  
1788 ues. Kahanpää et al. (2016) used these median winds to derive vortex diameters from mea-  
1789 sured pressure drop durations, assuming that the vortices moved with the velocity of the  
1790 background (median) wind. Resulting vortex diameters, encompassing pressure perturba-  
1791 tion exceeding 0.5 Pa, range from 2.3 m to 755 m, with a mean of 21 meters and median  
1792 of 16 meters. The distribution of these is similar to the distribution of dust devil diameters  
1793 observed by MER Spirit (Greeley et al. 2010).

1794 Solar irradiance loggers have been used terrestrially to detect obscuration of the Sun  
1795 resulting from dust within a dust devil (Lorenz and Jackson 2015). Compared to camera ob-  
1796 servations, solar irradiance measurements are better suited for long measurement campaigns  
1797 with fast sampling rate because of the reduced data volume and wider field of view. REMS'  
1798 ultraviolet (UV) sensor has been used for a similar survey on Mars (Zorzano et al. 2013).  
1799 REMS' six UV diodes measure downwelling solar flux in different spectral bands within an  
1800

## Field Measurements of Terrestrial and Martian Dust Devils

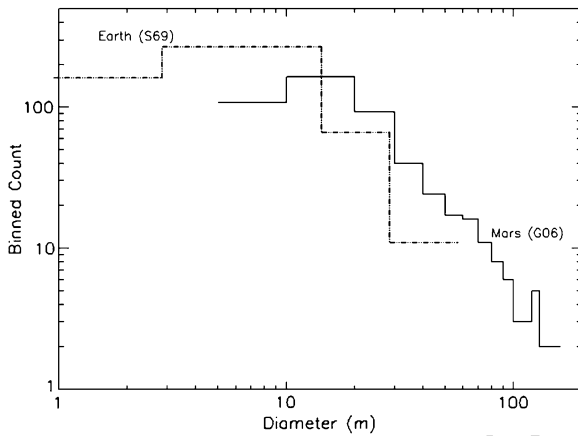


**Fig. 19** Differential diameter counts of dust devils from Sinclair's (1969) study at Tucson, and the martian Spirit observations of Greeley et al. (2006) involve roughly comparable survey areas. The roughly linear fall-off towards larger diameters on these logarithmic axes corresponds to a power-law diameter distribution; the turn-over at small diameters may indicate a minimum intrinsic size, or a poor detection efficiency for small devils. In this instance the modal diameter on Earth is more like 5 m, only a factor 3 smaller than on Mars. It is notable that the largest devil seen in the Mars set is larger than that at Earth, but perhaps a longer survey on Earth (pushing the curve upwards) would allow the expected number of detections of larger devils on Earth to rise above unity. As discussed in Lorenz and Jackson (2016) in this issue care must be exercised in drawing size population conclusions from different types of data due to observational biases, especially at the small size end of the distribution

upward facing 30-degree half-angle cone field-of-view (Gómez-Elvira et al. 2012). Observations of UV dips coincident with pressure dips are rare. Kahanpää et al. (2016) reported one very weak UV obscuration among its 252 pressure events. Steakley and Murphy (2016) identified 2 pressure events that appear to correspond to UV flux drops, but these pressure events cannot be confirmed as dust devils due to an instrumental error described in Harri et al. (2014) as the shadow effect. Although these events were eliminated from the sample, they may show signs of a double trough signature (Steakley and Murphy 2016) which could be produced by repeated passage into and out of the core of a cylindrical dust devil (Mason et al. 2013). Zorzano et al. (2013) searched for UV obscurations not concurrent with pressure dips, but found no clear signs of dust devils during MSL's first 100 sols. This lack of UV obscurations suggests that most or all vortices detected in the REMS pressure data are dustless, a result that agrees with the detection of only one dust devil by the MSL cameras (Moore et al. 2015).

## 4 Discussion

Despite the differing range of dust devils parameters measured by individual terrestrial campaigns, and their more extensive characterization than has been provided for martian dust devils, comparison between terrestrial and martian dust devils does indicate some differences and some similarities. Martian dust devils exhibit larger maximum widths and heights (Fig. 19) and faster maximum rotational wind speeds than their terrestrial counterparts (see Tables 1 and 2 and references therein). The more extreme inferred martian dust devil winds correspond to what is perceived to be the largest dust devils, which also correspond to the measurement location being most distant from the presumed core location.

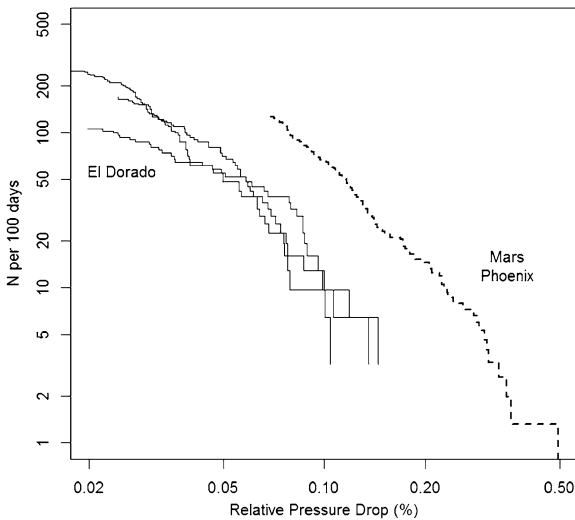


**Fig. 20** The number of times a vortex-induced pressure drop will be encountered by a fixed station on Earth and Mars is presented as a cumulative count. Because the absolute pressures on Mars are  $> 100$  times smaller than on Earth, it is more illuminating to use a relative pressure drop. Thus the ‘once a week’ vortex on Earth corresponds to about 0.1 % or 1 mbar pressure drop, while that on Mars is about 0.3 % or  $\sim 0.02$  mbar (2 Pa). Note that despite the differences in temperature and gas compositions between the two planets, the densities and pressures are approximately in the same proportion. Since the pressure drop of a vortex in cyclostrophic balance is  $\sim rV^2$ , then a fixed relative pressure drop corresponds roughly to a fixed maximum tangential speed  $V$  on both bodies: 0.1 % for a 10 m/s wind speed

Measured terrestrial maximum pressure drops are one order of magnitude larger than the measured maximum martian pressure drops. Renno et al. (1998, 2000) suggests that the potential pressure drop magnitude of a dust devil is proportional to the surface pressure. Since surface pressure on Earth is two orders of magnitude greater than on Mars, other aspects affecting potential vortex intensity, including the pressure thickness of the convective layer (‘boundary layer height’) and the near surface fraction of the mechanical dissipation of energy and the thermodynamic efficiency, must play a role in martian vortices only being one order of magnitude smaller in their depression than terrestrial dust devils. The larger observed size of martian dust devils (Fig. 1) could be one manifestation of these environmental characteristics.

The relative frequency of occurrence of both terrestrial and martian devils with a pressure drop magnitude,  $\Delta P$ , normalized by the local mean surface pressure exhibits a power law functional form (Fig. 20) represented by,  $\Delta P^{-x}$ , with  $x \sim 2$  (Lorenz 2012a, 2012b). A similar functional form for observed vortex diameter has also been proposed (Lorenz 2009), but an exponential fit has also been suggested, especially at smaller diameters (Fig. 19). These issues are more thoroughly explored in the accompanying papers by Lorenz and Jackson (2016) and Kurgansky et al. (2016).

Terrestrial field measurements have been obtained from numerous geographic locations and continents (Africa, Australia, North America, South America). There are some sites (Eldorado Valley, Nevada USA; Eloy, Arizona USA) that have served as the locales for a number of field campaigns. Martian measurements have also been obtained from discrete locations with a preference (5 of 7 successful missions) for equatorial/subtropical locations, though northern middle and polar latitudes have also been investigated. While mar-

1901 tian robotic missions do not offer the opportunity to upgrade or augment instrumentation  
1902 after launch (and often a substantial time period prior to launch), repeated terrestrial field  
1903 campaigns to the same location provide the possibility of building upon previous measure-  
1904 ments. A number of campaigns over 10–15 years at the Eldorado Valley site have used previ-  
1905 ously employed and accompanying new instrumentation (Metzger 1999; Balme et al. 2003;  
1906 Ringrose et al. 2007; Metzger et al. 2010, 2011; Balme et al. 2012; Mason et al. 2014;  
1907 Jackson and Lorenz 2015). These campaigns have employed mobile and deployable sta-  
1908 tionary measurement platforms, vertical masts with 10 meter heights to probe the vertical  
1909 structure of encountered dust devils, stereo camera imaging to improve quantification of  
1910 dust devil position and size, and recently networks of pressure loggers with partial cover-  
1911 age by solar flux loggers. None of the martian robotic missions to date have ‘returned’ to  
1912 a previous lander/rover location, and there is no pronounced motivation to do so for dust  
1913 devil measurements. One opportunity to do so could be realized with a Mars sample return  
1914 set of missions which could have a second spacecraft retrieve a sample previously cached  
1915 by a preliminary mission. If the preliminary mission’s measurements identified unique dust  
1916 devil characteristics at the cache site, possibly the cache retrieving mission could carry in-  
1917 strumentation to enhance characterization of the dust devils at the cache site, but mission  
1918 lead time development needs and other mission priorities would likely preclude such a an  
1919 instrumentation selection.

## 1920 **5 Future Dust Devil Measurements**

### 1921 **5.1 Earth**

1922 The basic features and correlations of properties of terrestrial dust devils have been mea-  
1923 sured, and somewhat robust statistics on the population are emerging. What is presently  
1924 lacking are data to support an evaluation of the dependence of dust devil morphology on  
1925 environmental parameters. For example, there is a somewhat anecdotal (see Chap. 6, Kur-  
1926 gansky et al. 2016) correlation of columnar vortices with very smooth land surfaces such as  
1927 playa, whereas rougher (e.g. scrubby) terrain tends to have more conical devils.

1928 Present profiles of dust devils do not allow discrimination of the various analytic func-  
1929 tions used as axisymmetric idealizations of vortex structure (Kurgansky et al. 2016). On the  
1930 other hand, it is not clear that better measurements will help, as it may be that nonideal-  
1931 ities are more significant than the difference between models. A prominent area that merits  
1932 further study is the frequency and nature of multi-cored vortices and what controls their  
1933 formation. Another deviation from axisymmetry is evident in simulations (e.g. Toigo et al.  
1934 2003)—that winds spiral into the vortex core in azimuthally-concentrated bands, like those  
1935 seen in hurricane clouds or in the arms of galaxies. Such azimuth variations have not yet  
1936 been formally documented in field observations. Finally, field measurements from Sinclair  
1937 (1973) and Lorenz (2012b) appear to show an asymmetry in the pressure profile of migrat-  
1938 ing dust devils, the ‘attack’ slope being shallower than the ‘decay’. This may be a generic  
1939 feature of a migrating vortex, tilted by wind shear, but has not been quantified.

1940 Another question is the possible role in dust devil energy balance of sunlight intercepted  
1941 by lofted dust. It is sometimes noticed that devils become more intense when they become  
1942 dustier—but is this cause, or effect? If effect, is it sensible heat in the dust and air pulled  
1943 off the ground, or is the solar heat introduced by the absorbing dust and introduced into the  
1944 vortex directly a significant factor? Field measurements, perhaps including thermal as well  
1945 as video imaging (to relate flow speeds to dust temperature) may illuminate this question.

1951 Related to this question is that of dust-lifting per-se: do larger, more vigorous, but less fre-  
1952 quently occurring, dust devils lift more dust than smaller, more numerous ones? Can the dust  
1953 lifting of a dust devil ever be disentangled from the properties of the surface (i.e. is the dusti-  
1954 ness of a dust devil controlled mainly by surface properties or by its internal properties?).  
1955 Only by coordinated measurements of dust content and wind speed (likely in-situ measure-  
1956 ment), and dust devil diameter (likely remote measurements) from controlled field-sites can  
1957 these questions be addressed. Such measurements would help provide better understanding  
1958 of the environmental effects of dust devils and provide a model for comparison with Mars.

1959 Circumstantial observations, dating as far back as Flower (1936) and a correlation of  
1960 satellite-observed dust devil heights and estimates of planetary boundary layer thickness  
1961 from model predictions and occultation measurements (Fenton and Lorenz 2015) suggest  
1962 dust devil heights and spacings may be controlled by the planetary boundary layer (PBL)  
1963 thickness. In-situ measurements that establish this correlation more securely (perhaps also  
1964 validating the anecdotal suggestion that small devils are more common early in the day  
1965 and larger ones in the late afternoon, consistent with the diurnal growth of the PBL) would  
1966 similarly be useful.

1967 In summary, terrestrial dust devil characterization would benefit from dedicated cam-  
1968 paigns of long-lived networks of uniformly instrumented stations measuring pressure, wind  
1969 (3-D), temperature, dust load, electric field, etc. Measurements at a variety of heights above  
1970 the surface would be valuable. High cadence (1 Hz) measurements in conjunction with imag-  
1971 ing of the network would aid in correlating visible dust devil manifestation with interior  
1972 conditions. The use of several networks in dissimilar field sites would enable the influence  
1973 of local surface properties to be disentangled from the properties of individual dust devils.

## 1974 5.2 Mars

1975 Measurement characterization of martian dust devils is limited by the scarcity of observa-  
1976 tions, especially those that provide simultaneous measurements of a variety of geophysical  
1977 parameters. Since dust devils play a substantial role in maintaining Mars' persistent dust  
1978 haze, especially during the aphelion season, better characterizing their attributes will enable  
1979 improved understanding of their role in providing/maintaining the thermodynamically  
1980 important atmospheric dust load.

1981 Robotic spacecraft sent to Mars' surface should carry imaging systems capable of pro-  
1982 viding high resolution and fast frame rates covering a wide field of view. Monochrome  
1983 imaging is adequate (Greeley et al. 2010) and would not interfere with other onboard color  
1984 imagers dedicated to geologic studies. An imaging system that provides full azimuthal cov-  
1985 erage and onboard software to identify and retain images that display dust devil diagnostic  
1986 temporal variability (thus reducing downlink volume of dust-devil deficient images) would  
1987 enable greater temporal coverage than has been provided previously. The dust-devil imaging  
1988 strategy employed by Spirit (and Opportunity) Navigation Cameras did provide substantial  
1989 numbers of dust devil observations, targeted to the times of sol when they were most fre-  
1990 quent.

1991 No robotic spacecraft has yet provided unambiguous contemporaneous measurement of  
1992 surface pressure and wind. Thus, the dynamic connection between vortex magnitude and  
1993 velocity fields has not been established. Hot wire / hot film anemometers have been the  
1994 only type of high-frequency sampling wind instruments to operate on Mars' surface, and  
1995 all have suffered from instrument failure and/or calibration difficulties and placement is-  
1996 sues (Lenoir et al. 2011; Lorenz and Sotzen 2014). These instruments have generally been  
1997 low mass, which are desirable, but their poor performance record suggests other sensor  
1998  
1999  
2000

types might be warranted. An enhanced REMS wind sensor is selected for NASA's InSight lander (scheduled for a 2018 launch). NASA's 2020 Mars Rover will carry a meteorology package (Rodríguez-Manfredi et al. 2014). Acoustic and laser Doppler anemometers have been suggested as possible technologies applicable for Mars (Merrison et al. 2006; Wilson et al. 2008; Esposito 2011; Banfield 2012; Leonard-Pugh et al. 2012; Rafkin et al. 2013). Both technologies enable high frequency sampling, 10 Hz or more, of the three-dimensional wind field, which provides opportunity for determination of turbulent characteristics of the flow. Acoustic anemometry has the added advantage of providing simultaneous atmospheric temperature measurement which when coupled to the winds affords quantification of the turbulent thermal flux. To date neither technology has been selected for flight. Wind socks provide wind sampling at very low frequencies (Sullivan et al. 2000; Holstein-Rathlou et al. 2010), but their data bandwidth requirement is large compared to their low response time and inability to unambiguously provide the vertical wind component.

Pressure measurements have provided the most valuable and plentiful in situ dust devil/convective vortex measurements to date. The high resolution (0.1–0.2 Pa) and high sampling frequencies (2–0.25 Hz) implemented have proved adequate to capture pressure signatures. Care must be taken for future opportunities to avoid sensor thermal variation which complicates pressure value determination, as well as inlet orientation which can provide unfavorable dynamic pressure contamination, and measurement tube length/diameter which affects sensor response time (Ellehoj et al. 2010). The low power and mass requirements of the necessary equipment as well as the tremendous value of martian surface pressure measurements for both local (dust devil) and larger scale atmospheric analyses warrant pressure sensors being included on every robotic spacecraft landed upon Mars' surface.

Contemporaneous measurement of received solar flux and pressure/wind signatures of vortex passage are necessary to assess the 'dustiness' of vortices and thus the frequency of occurrence of dust devils vs. 'clear' convective vortices. Such discrimination would aid the assessment of vortex thermal vs. dust vertical fluxes. Dedicated solar flux instruments can provide appropriate measurements (Gómez-Elvira et al. 2012; Kahanpää et al. 2016) with a cadence coupled to that of other science instruments. Engineering systems can also provide solar flux measurements at no additional 'cost' (Schofield et al. 1997), though likely at a lower cadence than desired for science purposes.

To date no martian robotic lander/rover has provided electric field or dust concentration or dust particle flux/size distribution measurements. ESA's Schiaparelli lander's MicroARES system will provide initial electric field measurements during that missions short duration operations in late 2016 (Esposito et al. 2016a, 2016b). A laser Doppler anemometer could provide particle concentration in addition to velocity, but as previously stated no such instrument is currently selected for a Mars robotic mission. A vertically oriented LIDAR system onboard the NASA Phoenix lander provided vertical resolution of aerosol concentration within the bottom few kilometers of the atmosphere (Whiteway et al. 2008). A horizontally scanning LIDAR system could provide signals from which radial variations in near-surface aerosol abundance within several kilometers of a lander/rover could be obtained.

Dust devil infrasound/acoustic and seismic measurements are still minimally available for terrestrial studies, and their full diagnostic value remains immature yet promising; a seismometer, for example, appears to be capable of tracking close encounters with dust devils, recovering an estimate of the azimuth history and constraining the integral of the pressure field (relating to diameter and core pressure drop). In combination with wind and pressure measurements, the dust devil parameters and miss distance may be reconstructed or at least constrained (Lorenz et al. 2015a). The NASA InSight mission will provide meteorological

and seismic measurements that will improve understanding of dust devils for both martian and terrestrial applications. In addition, the seismic signals of dust devils may also provide information about the surface and subsurface properties at the InSight landing site by acting as calibration loads (Lorenz et al. 2015a, 2015b). A Mars microphone is going to be part of the payload of the 2018 Exomars landing platform (Zelenyi et al. 2015). The microphone, with a bandwidth of 100 Hz à 10 kHz, will record, for the first time, audio signals at the surface of Mars and is expected to contribute to atmospheric science investigations including dust devil studies (Maurice et al. 2016).

Ideally a network of meteorologically outfitted stations designed to characterize dust devils will be deployed upon Mars' surface within a very limited spatial footprint, possibly as one component of a more globally extensive network. The PASCAL network mission developed and proposed to from NASA Ames in the late 1990's/early 2000's developed some network concepts but was not selected to launch.

## 6 Conclusions

Dust devils are inherently difficult to measure. Their occurrence is somewhat unpredictable in both space and time and they are fast-moving, short-lived phenomena. Observational 'survey' data have provided information about size-frequency distributions, sense of rotation and other parameters, but to assess the wind and pressure structure, and the dust-loading behaviour of a dust devil has required in-situ measurement.

To obtain these data, terrestrial dust devils have either been "chased" or "monitored". The former method can be subject to observation bias, but the latter can require long field campaigns and multiple sets of instruments if statistically significant numbers of data are to be obtained. Recently, advances in both instrumentation and data recording technology have enabled new methodologies to be developed to solve these problems. Long-term, high cadence monitoring using multiple sensors, coupled with automatically controlled imaging provides a way to get the 'best of both worlds'. In the next ten years, new field studies should be able to provide much better data about population-statistics of dust devils and their environmental role.

On Mars, dust devils studies have generally 'piggy-backed' on other camera or meteorological studies. Nevertheless, significant progress in measuring population statistics and pressure-structure have been possible. These data have been complemented by remote-sensing observations from orbit—a method not widely applied on Earth.

Future studies for Mars should focus on in situ, high cadence sampling of pressure, wind speed and dust load. Along with the continuing operation of the US/NASA MSL Curiosity rover, the next opportunity for martian dust devil measurements will be provided by the ESA/Russian ExoMars Schiaparelli Lander scheduled for ~ 1 week's operation on Mars surface during late 2016. The longer lived US/NASA InSight lander is scheduled to arrive in late 2018, followed by the ESA ExoMars Rover and the US/NASA 2020 Rover in early 2021.

**Acknowledgements** All authors thank the International Space Science Institute for organizing and hosting the February 2015 Bern, Switzerland Workshop and for providing lodging accommodations. J. Murphy thanks the New Mexico State University College of Arts & Sciences Faculty Travel Award program for travel support. K. Steakley thanks the New Mexico State University (NMSU) Aggies Go Global organization, NMSU Graduate School, Associated Students of NMSU, New Mexico Space Grant Consortium, and NMSU Astronomy Department for funding support. M. Balme acknowledges funding from the UK Space Agency (grant ST/L00643X/1) and from STFC, the UK Science and Technology Facilities Council (grant ST/L000776/1). R. Lorenz acknowledges the support of NASA Mars Fundamental Research Program Grant

2101 NNX12AI04G. N. Murdoch was supported by a CNES-provided Post-doctoral award. M. Patel acknowl-  
2102 edges support from the UK STFC and UK Space Agency under grants ST/T003061/1 and ST/P001262/1  
2103 and as part of the project UPWARDS-633127, funded by the European Union's Horizon 2020 Programme  
2104 (H2020-Compet-08-2014). P. Whelley was supported by the NASA Post Doctoral Program and NASA's *Re-*  
2105 *mote, In Situ, and Synchrotron Studies for Science and Exploration* project.

2106 The authors thank two anonymous reviewers for their thorough evaluations which have resulted in an  
2107 improved final paper.

## 2108 References

- 2109 R.A. Bagnold, *The Physics of Blown Sand and Desert Dunes* (Dover, Mineola, 1941)
- 2110 M.R. Balme, A. Pathare, S.M. Metzger, M.C. Towner, S.R. Lewis, A. Spiga, L.K. Fenton, N.O. Renno, H.M.  
2111 Elliott, F.A. Saca, T.I. Michaels, P. Russell, J. Verdasca, Field measurements of horizontal forward  
2112 motion velocities of terrestrial dust devils: towards a proxy for ambient winds on Mars and Earth. *Icarus*  
2113 **221**(2), 632–645 (2012)
- 2114 M. Balme, R. Greeley, Dust devils on Earth and Mars. *Rev. Geophys.* **44**, RG3003 (2006)
- 2115 M. Balme, S. Metzger, M. Towner, T. Ringrose, R. Greeley, J. Iversen, Friction wind speeds in dust devils:  
2116 a field study. *Geophys. Res. Lett.* **30**(16), 1830 (2003). doi:[10.1029/2003GL017493](https://doi.org/10.1029/2003GL017493)
- 2117 D. Banfield, Mars acoustic anemometer, *AGU Fall Meeting 2012*, San Francisco, California, USA. Poster  
2118 presentation (2012), <http://abstractsearch.agu.org/meetings/2012/FM/P23A-1916.html>
- 2119 D. Banfield, Atmospheric observations from the Mars insight mission, in *Fifth International Workshop on*  
2120 *the Mars Atmosphere: Modelling and Observations*, Oxford, UK (2014). Oral presentation, [http://](http://www-mars.lmd.jussieu.fr/oxford2014/abstracts/banfield_oxford2014.pdf)  
2121 [www-mars.lmd.jussieu.fr/oxford2014/abstracts/banfield\\_oxford2014.pdf](http://www-mars.lmd.jussieu.fr/oxford2014/abstracts/banfield_oxford2014.pdf)
- 2122 A.J. Bedard, Low frequency atmospheric acoustic energy associated with vortices produced by thunder-  
2123 storms. *Mon. Weather Rev.* 241–243 (2005)
- 2124 F. Bell, Dust devils and aviation, report, *Meteorol. Note 27*, Aust. Bur. of Meteorol., Melbourne, Victoria,  
2125 1967
- 2126 J.-J. Berthelier, ARES, atmospheric relaxation and electric field sensor, the electric field experiment on NET-  
2127 LANDER. *Planet. Space Sci.* **48**(12–14), 1193–2000 (2000)
- 2128 C. Bettanini et al., The DREAMS experiment on the ExoMars 2016 mission for the study of martian  
2129 environment during the dust storm season. *MetroAeroSpace* **167**(173), 29–30 (2014). doi:[10.1109/](https://doi.org/10.1109/MetroAeroSpace.2014.6865914)  
2130 [MetroAeroSpace.2014.6865914](https://doi.org/10.1109/MetroAeroSpace.2014.6865914)
- 2131 H.B. Bluestein, A.L. Pazmany, Observations of tornadoes and other convective phenomena with a mobile,  
2132 3-mm wavelength, Doppler radar: the spring 1999 field experiment. *Bull. Am. Meteorol. Soc.* **81**, 2939–  
2133 2951 (2000)
- 2134 J.J. Carroll, J.A. Ryan, Atmospheric vorticity and dust devil rotation. *J. Geophys. Res.* **75**, 5179–5184 (1970)
- 2135 W.D. Crozier, Dust devil properties. *J. Geophys. Res.* **75**, 4583–4585 (1970)
- 2136 R. Davy, J.A. Davies, P.A. Taylor, C. Lange, W. Weng, J. Whiteway, H.P. Gunnlaugson, Initial analysis of air  
2137 temperature and related data from the Phoenix MET station and their use in estimating turbulent heat  
2138 fluxes. *J. Geophys. Res.* **115**, E00E13 (2010). doi:[10.1029/2009JE003444](https://doi.org/10.1029/2009JE003444)
- 2139 S.J. Desch, J.N. Cuzzi, The generation of lightning in the solar nebula. *Icarus* **143**, 87–105 (2000). doi:  
2140 [10.1006/icar.1999.6245](https://doi.org/10.1006/icar.1999.6245)
- 2141 M. Domínguez, V. Jiménez, J. Ricart, L. Kowalski, J. Torres, S. Navarro, J. Romeral, L. Castañer, A hot  
2142 film anemometer for the martian atmosphere. *Planet. Space Sci.* **56**(8), 1169–1179 (2008). doi:[10.1016/](https://doi.org/10.1016/j.jplss.2008.02.013)  
2143 [j.jplss.2008.02.013](https://doi.org/10.1016/j.jplss.2008.02.013)
- 2144 N. Duff, D.J. Lacks, Particle dynamics simulations of triboelectric charging in granular insulator systems.  
2145 *J. Electrostat.* **66**, 51 (2008). doi:[10.1016/j.elstat.2007.08.005](https://doi.org/10.1016/j.elstat.2007.08.005)
- 2146 R. Edmonds, Examination of two martian atmosphere phenomena: dust devil acoustics and gravity wave  
2147 forcing of dust storm development. PhD dissertation, New Mexico State University, 2014, p. 223
- 2148 M.D. Ellehoj, H.P. Gunnlaugsson, P.A. Taylor, H. Kahanpää, K.M. Bean, B.A. Cantor, B.T. Gheynani, L.  
2149 Drube, D. Fisher, A.-M. Harri, C. Holstein-Rathlou, M.T. Lemmon, M.B. Madsen, M.C. Malin, J.  
2150 Polkko, P.H. Smith, L.K. Tamppari, W. Weng, J. Whiteway, Convective vortices and dust devils as the  
2151 Phoenix Mars mission landing site. *J. Geophys. Res.* **115**, E00E16 (2010). doi:[10.1029/2009JE003413](https://doi.org/10.1029/2009JE003413)
- 2152 F. Esposito, MEDUSA: observation of atmospheric dust and water vapor close to the surface of Mars. *Mars*  
2153 **6**, 1–12 (2011). <http://www.marsjournal.org/contents/2011/0001/>. doi:[10.1555/mars.2011.0001](https://doi.org/10.1555/mars.2011.0001)
- 2154 F. Esposito et al., The role of the atmospheric electric field in the dust-lifting process. *Geophys. Res. Lett.* **43**  
2155 (2016a). doi:[10.1002/2011GL068463](https://doi.org/10.1002/2011GL068463)
- 2156 F. Esposito, R. Molinaro, G.I. Popa, C. Molfese, F. Cozzolino, L. Marty, K. Taj-Eddine, G. Di Achille, G.  
2157 Franzese, S. Silvestro, G.C. Ori, The role of atmospheric electric field in the dust lifting process. *Geo-*  
2158 *phys. Res. Lett.* (2016b, in press)

- 2151 L.K. Fenton, R. Lorenz, Dust devil height and spacing with relation to the martian planetary boundary layer  
2152 thickness. *Icarus* **260**, 246–262 (2015). doi:[10.1016/j.icarus.2015.07.028](https://doi.org/10.1016/j.icarus.2015.07.028)
- 2153 L. Fenton, D. Reiss, M. Lemmon, B. Marticorena, S. Lewis, B. Cantor, Orbital observations of dust lofted by  
2154 daytime convective turbulence. *Space Sci. Rev.* (2016). doi:[10.1007/s11214-016-0243-6](https://doi.org/10.1007/s11214-016-0243-6)
- 2155 F. Ferri, P.H. Smith, M.T. Lemmon, N. Renno, Dust devils as observed by Mars Pathfinder. *J. Geophys. Res.*  
2156 **108**(E12), 5133 (2003). doi:[10.1029/2000JE001421](https://doi.org/10.1029/2000JE001421)
- 2157 D.E. Fitzjarrald, A field investigation of dust devils. *J. Appl. Meteorol.* **12**, 808–813 (1973)
- 2158 W.D. Flower, Sand devils. *Lond. Meteorol. Off. Prof. Notes* **5**(71), 1–16 (1936)
- 2159 K.M. Forward, D.J. Lacks, R.M. Sankaran, Particle-size dependent bipolar charging of martian regolith sim-  
2160 ulant. *Geophys. Res. Lett.* **36**(13), L13201 (2009)
- 2161 G.D. Freier, The electric field of a large dust devil. *J. Geophys. Res.* **65**, 3504 (1960). doi:[10.1029/  
2162 JZ065i010p03504](https://doi.org/10.1029/JZ065i010p03504)
- 2163 S.D. Fuerstenau, Solar heating of suspended particles and the dynamics of martian dust devils. *Geophys. Res.*  
2164 *Lett.* **33**, 19 (2006). doi:[10.1029/2006GL026798](https://doi.org/10.1029/2006GL026798)
- 2165 E.W.B. Gill, Friction electrification of sand. *Nature* **162**, 568 (1948)
- 2166 D.A. Gillette, P. Sinclair, Estimation of suspension of alkaline material by dust devils in the United States.  
2167 *Atmos. Environ.* **24**(A), 1135–1142 (1990)
- 2168 D.A. Gillette, I.H. Blifford, D.W. Fryrear, Influence of wind velocity on size distributions of aerosols gener-  
2169 ated by wind erosion of soils. *J. Geophys. Res.* **79**, 4068–4075 (1974)
- 2170 M. Golombek et al., Overview of the Mars Pathfinder mission and assessment of landing site predictions.  
2171 *Science* **278**, 5344 (1997). doi:[10.1126/science.278.5344.1743](https://doi.org/10.1126/science.278.5344.1743)
- 2172 J. Gómez-Elvira et al., REMS: the environmental sensor suite for the Mars science laboratory rover. *Space*  
2173 *Sci. Rev.* **170**, 583–640 (2012). doi:[10.1007/s11214-012-9921-1](https://doi.org/10.1007/s11214-012-9921-1)
- 2174 J. Gómez-Elvira et al., Curiosity’s rover environmental monitoring station: overview of the first 100 sols.  
2175 *J. Geophys. Res., Planets* **119**, 1680–1688 (2014). doi:[10.1002/2013JE004576](https://doi.org/10.1002/2013JE004576)
- 2176 C.G. Grant, Dust devils in the sub-arctic. *Weather* **4**, 402–403 (1949)
- 2177 R. Greeley, J.D. Iversen, *Wind as a Geological Process*. Cambridge Planetary Science Series (Cambridge  
2178 University Press, Cambridge, 1985). ISBN 0521356927
- 2179 R. Greeley et al., Wind related features in Gusev crater, Mars. *J. Geophys. Res.* **108**(E12), 8077 (2003)
- 2180 R. Greeley, P.L. Whelley, R.E. Arvidson, N.A. Cabrol, D.J. Foley, B.J. Franklin, P.G. Geissler, M.P.  
2181 Golombek, R.O. Kuzmin, G.A. Landis, M.T. Lemmon, L.D.V. Neakrase, S.W. Squyres, S.D. Thomp-  
2182 son, Active dust devils in Gusev Crater, Mars: observations from the Mars exploration rover spirit.  
2183 *J. Geophys. Res.* **111**(E12) (2006). doi:[10.1029/2006JE002743](https://doi.org/10.1029/2006JE002743)
- 2184 R. Greeley, D.A. Waller, N.A. Cabrol, G.A. Landis, M.T. Lemmon, L.V. Neakrase, M. Pendelton Hoffer, S.D.  
2185 Thompson, Gusev Crater, Mars: observations of three dust devil seasons. *J. Geophys. Res.* **115** (2010)
- 2186 J. Grotzinger et al., Mars science laboratory mission and science investigation. *Space Sci. Rev.* **170**(1), 5–56  
2187 (2012). doi:[10.1007/s11214-012-9892-2](https://doi.org/10.1007/s11214-012-9892-2)
- 2188 H.P. Gunnlaugsson et al., Telltale wind indicator for the Mars Phoenix lander. *J. Geophys. Res.* **113**, E00A04  
2189 (2008). doi:[10.1029/2007JE003008](https://doi.org/10.1029/2007JE003008)
- 2190 R.M. Haberle, J. Gómez-Elvira, M. de la Torre Juárez, A.-M. Harri, J.L. Hollingsworth, H. Kahanpää, M.A.  
2191 Kahre, M. Lemmon, F.J. Martín-Torres, M. Mischna, J.E. Moores, C. Newman, S.C.R. Rafkin, N.  
2192 Rennó, M.I. Richardson, J.A. Rodríguez-Manfredi, A.R. Vasavada, M.-P. Zorzano-Mier, REMS/MSL  
2193 Science Teams, Preliminary interpretation of the REMS pressure data from the first 100 sols of the MSL  
2194 mission. *J. Geophys. Res., Planets* **119**, 440–453 (2014). doi:[10.1002/2013JE004488](https://doi.org/10.1002/2013JE004488)
- 2195 J. Hallett, T. Hoffer, Dust devil systems. *Weather* **26**, 247–250 (1971)
- 2196 W.R. Harper, *Contact and Frictional Dissipation* (Clarendon Press, Oxford, 1967)
- 2197 A.-M. Harri, M. Genzer, O. Kempainen, H. Kahanpää, J. Gomez-Elvira, J.A. Rodriguez-Manfredi, R.  
2198 Haberle, J. Polkko, W. Schmidt, H. Savijärvi, J. Kauhanen, E. Atlaskin, M. Richardson, T. Siili, M.  
2199 Paton, M. de la Torre Juarez, C. Newman, S. Rafkin, M.T. Lemmon, M. Mischna, S. Merikallio, H.  
2200 Haukka, J. Martin-Torres, M.-P. Zorzano, V. Peinado, R. Urqui, A. Lapinette, A. Scodary, T. Mäkinen,  
L. Vazquez, N. Rennó, The REMS/MSL Science Team, Pressure observations by the curiosity rover:  
initial results. *J. Geophys. Res., Planets* **119**, 82–92 (2014). doi:[10.1002/2013JE004423](https://doi.org/10.1002/2013JE004423)
- 2199 R.G. Harrison, E. Barth, F. Esposito, J. Merrison, F. Montmessin, K.L. Aplin, C. Borlina, J.J. Berthelier,  
2200 G. Déprez, W.M. Farrell, I.M.P. Houghton, N.O. Renno, K.A. Nicoll, S.N. Tripathi, M. Zimmerman,  
Applications of electrified dust and dust devil electrodynamic to martian atmospheric electricity. *Space*  
*Sci. Rev.* (2016). doi:[10.1007/s11214-016-0241-8](https://doi.org/10.1007/s11214-016-0241-8)
- 2197 M. Hecht, M.D. Pratt, D. Catling, S. Samulon, MATADOR dust devil campaign (2001)
- 2198 G.D. Hess, K.T. Spillane, Characteristics of dust devils in Australia. *J. Appl. Meteorol.* **29**, 498–507 (1990)
- 2199 S.L. Hess, R.M. Henry, C.B. Leovy, J.A. Ryan, J.E. Tillman, Meteorological results from the surface of Mars:  
viking 1 and 2. *J. Geophys. Res.* **82**(28), 4559–4574 (1977). doi:[10.1029/J082i028p04559](https://doi.org/10.1029/J082i028p04559)

Field Measurements of Terrestrial and Martian Dust Devils

- 2201 C. Holstein-Rathlou et al., Winds at the Phoenix landing site. *J. Geophys. Res.* **115**, E00E18 (2010). doi:  
2202 [10.1029/2009JE003411](https://doi.org/10.1029/2009JE003411)
- 2203 R.G. Horn, D.T. Smith, A. Grabbe, Contact electrification induced by monolayer modification of a surface  
2204 and relation to acid-base interactions. *Nature* **366**, 442–443 (1993). doi:[10.1038/366442a0](https://doi.org/10.1038/366442a0)
- 2205 M.S. Howe, *Theory of Vortex Sound* (Cambridge University Press, Cambridge, 2003)
- 2206 I.I. Inculet, G.S.P. Castle, G. Aartsen, Generation of bipolar electric fields during industrial handling of pow-  
2207 ders. *Chem. Eng. Sci.* **61**, 2249–2253 (2006). doi:[10.1016/j.ces.2005.05.005](https://doi.org/10.1016/j.ces.2005.05.005)
- 2208 J. Ito, H. Niino, Particle image velocimetry of a dust devil observed in a desert. *Sci. Online Lett. Atmos.*  
2209 **10**(1), 108–111 (2014)
- 2210 R.L. Ives, Behavior of dust devils. *Bull. Am. Meteorol. Soc.* **28**, 168–174 (1947)
- 2211 D.J. Lacks, A. Levandovsky, Effect of particle size distribution on the polarity of triboelectric charging in  
2212 granular insulator systems. *J. Electrostat.* **65**, 107 (2007)
- 2213 T.L. Jackson, W.M. Farrell, *IEEE Trans. Geosci. Remote Sens.* **44**, 2942 (2006). doi:[10.1109/TGRS.2006.](https://doi.org/10.1109/TGRS.2006.875785)  
2214 [875785](https://doi.org/10.1109/TGRS.2006.875785)
- 2215 B. Jackson, R. Lorenz, A multiyear dust devil vortex survey using an automated search of pressure time  
2216 series. *J. Geophys. Res.* **120**(2), 401–412 (2015). doi:[10.1092/2014JE004712](https://doi.org/10.1092/2014JE004712)
- 2217 H. Kahanpää, C. Newman, J. Moores, M-P. Zorzano, J. Martín-Torres, S. Navarro, A. Lepinette, M.T. Lem-  
2218 mon, B. Cantor, P. Valentín-Serrano, A. Ullán, W. Schmidt, Convective vortices and dust devils at the  
2219 MSL landing site: annual variability. *J. Geophys. Res. Planets* **121** (2016). doi:[10.1002/2016JE005027](https://doi.org/10.1002/2016JE005027)
- 2220 M. Kahre, J. Murphy, R. Haberle, Modeling the martian dust cycle and surface dust reservoirs with the NASA  
2221 Ames general circulation model. *J. Geophys. Res., Planets* **111**, E6 (2006)
- 2222 J.C. Kaimal, J.A. Bussinger, Case studies of a convective plume and a dust devil. *J. Appl. Meteorol.* **9**, 612–  
2223 620 (1970)
- 2224 M. Klose, B.C. Jemmet-Smith, H. Kahanpää, M. Kahre, P. Knippertz, M. Lemmon, S. Lewis, R. Lorenz, L.  
2225 Neakrase, C. Newman, M. Patel, D. Reiss, A. Spioga, P. Whelley, *Space Sci. Rev.* (2016). doi:[10.1007/](https://doi.org/10.1007/s11214-016-0261-4)  
2226 [s11214-016-0261-4](https://doi.org/10.1007/s11214-016-0261-4)
- 2227 J.F. Kok, N.O. Renno, Enhancement of the emission of mineral dust aerosols by electric forces. *Geophys.*  
2228 *Res. Lett.* **33**, L19S10 (2006)
- 2229 J.F. Kok, N.O. Renno, Electrostatics in wind-blown sand. *Phys. Rev. Lett.* **100**, 014501 (2008)
- 2230 M.V. Kurgansky, Size distribution of dust devils in the atmosphere. *Izv., Atmos. Ocean. Phys.* **42**(3), 319–325  
2231 (2006)
- 2232 Kurgansky et al., Dust devil steady-state structure from a fluid dynamic perspective. *Space Sci. Rev.* (2016,  
2233 in revision)
- 2234 M.V. Kurgansky, A. Montecinos, V. Villagran, S.M. Metzger, Micrometeorological conditions for dust-  
2235 devil occurrence in the Atacama Desert. *Bound.-Layer Meteorol.* **138**, 285–298 (2011). doi:[10.1007/](https://doi.org/10.1007/s10546-010-9549-1)  
2236 [s10546-010-9549-1](https://doi.org/10.1007/s10546-010-9549-1)
- 2237 R.I. Lambeth, On the measurement of dust devil parameters. *Bull. Am. Meteorol. Soc.* **47**, 522–526 (1966)
- 2238 G.A. Landis, P.P. Jenkins, Measurement of the settling rate of atmospheric dust on Mars by the MAE instru-  
2239 ment on Mars Pathfinder. *J. Geophys. Res.* **105**(E1), 1855–1857 (2000). doi:[10.1029/1999JE001029](https://doi.org/10.1029/1999JE001029)
- 2240 J. Latham, The electrification of snowstorms and sandstorms. *Q. J. R. Meteorol. Soc.* **90**, 383 (1964). doi:  
2241 [10.1002/qj.49709038310](https://doi.org/10.1002/qj.49709038310)
- 2242 J. Latham, C.D. Stow, A laboratory investigation of the electrification of snowstorms. *Q. J. R. Meteorol. Soc.*  
2243 **94**, 415 (1968)
- 2244 M.T. Lemmon, M.J. Wolff, M.D. Smith, R.T. Clancy, D. Banfield, G.A. Landis, A. Ghosh, P.H. Smith,  
2245 N. Spanovich, B. Whitney, P. Whelley, R. Greeley, S. Thompson, J.F. Bell III, S.W. Squyres, Atmo-  
2246 spheric imaging results from the Mars exploration rovers: spirit and opportunity. *Science* **306**, 1753–  
2247 1756 (2004)
- 2248 M.T. Lemmon, M.J. Wolff, J.F. Bell III., M.D. Smith, B.A. Cantor, P.H. Smith, Dust aerosol, clouds and the  
2249 atmospheric optical depth record over 5 Mars years of the Mars exploration rover mission. *Icarus* **251**,  
2250 96–111 (2015)
- 2251 B. Lenoir, D. Banfield, D.A. Caughey, Accommodation study for an anemometer on a martian lander. *J. At-  
2252 mos. Ocean. Technol.* **28**, 210–218 (2011). doi:[10.1175/2010JTECHA1490.1](https://doi.org/10.1175/2010JTECHA1490.1)
- 2253 E. Leonard-Pugh, C. Wilson, S. Calcutt, L. Davis, Capacitive ultrasonic transducer development for acous-  
2254 tic anemometry on Mars in *44th Annual Meeting of the Division for Planetary Sciences of the Amer-  
2255 ican Astronomical Society*, Reno, NV, USA (2012). Poster presentation, [http://adsabs.harvard.edu/](http://adsabs.harvard.edu/abs/2012DPS...4421523L)  
[abs/2012DPS...4421523L](http://adsabs.harvard.edu/abs/2012DPS...4421523L)
- 2256 P. Lognonné, B. Mosser, Planetary seismology. *Surv. Geophys.* **14**, 239–302 (1993)
- 2257 P. Lognonné, W.B. Banerdt, K. Hurst, D. Mimoun, R. Garcia, M. Lefeuvre, J. Gagnepain-Beyneix, M. Wic-  
2258 zorek, A. Mocquet, M. Panning, E. Beucler, S. Deraucourt, D. Giardini, L. Boschi, U. Christensen, W.  
2259 Goetz, T. Pike, C. Johnson, R. Weber, K. Larmat, N. Kobayashi, J. Tromp, Insight and single-station  
2260 broadband seismology: from signal and noise to interior structure determination, in *43rd Lunar and  
2261 Planetary Science Conference*, Houston, TX, March 2012 (2012). Abstract #1983

- 2251 R. Lorenz, Thermal imaging of a desert dust devil. *J. Meteorol.* **29**(292), 275–276 (2004)
- 2252 R.D. Lorenz, Power law of dust devil diameters on Mars and Earth. *Icarus* **203**(2), 683–684 (2009)
- 2253 R. Lorenz, On the statistical distribution of dust devil diameter. *Icarus* **215**(1), 381–390 (2011)
- 2254 R.D. Lorenz, Power law distribution of pressure drops in dust devils: observation techniques and Earth–Mars comparison. *Planet. Space Sci.* **60**, 370–375 (2012a). doi:[10.1016/j.pss.2011.11.003](https://doi.org/10.1016/j.pss.2011.11.003)
- 2255 R.D. Lorenz, Observing desert dust devils with a pressure logger. *Geosci. Instrum. Method. Data Syst.* **1**, 209–220 (2012b)
- 2256 R. Lorenz, The longevity and aspect ratio of dust devils: effects on detection efficiencies and comparison of landed and orbital imaging at Mars. *Icarus* **226**, 964–970 (2013)
- 2257 R.D. Lorenz, Vortex encounter rates with fixed barometer stations: comparison with visual dust devil counts and large eddy simulations. *J. Atmos. Sci.* **71**, 4461–4472 (2014) <uncited>
- 2258 R.D. Lorenz, Heuristic estimation of dust devil vortex parameters and trajectories from single-station meteorological observations: application to InSight at Mars. *Icarus* **271**(2–16), 326–337 (2016)
- 2259 R.D. Lorenz, D. Christie, Dust devil signatures in infrasound records of the international monitoring system. *Geophys. Res. Lett.* **42**(6), 2009–2014 (2015)
- 2260 R.D. Lorenz, B.K. Jackson, Dust devils and dustless vortices on a desert playa observed with surface pressure and solar flux logging. *GeoResJ* **5**, 1–11 (2015). doi:[10.1016/j.grj.2014.11.002](https://doi.org/10.1016/j.grj.2014.11.002)
- 2261 R.D. Lorenz, B. Jackson, Dust devil populations and statistics. *Space Sci. Rev.* (2016). doi:[10.1007/s11214-016-0277-9](https://doi.org/10.1007/s11214-016-0277-9)
- 2262 R.D. Lorenz, P.D. Lanagan, A barometric survey of dust devil vortices on a desert playa. *Bound.-Layer Meteorol.* **53**, 555–568 (2014). doi:[10.1007/s10546-014-9954-y](https://doi.org/10.1007/s10546-014-9954-y)
- 2263 R. Lorenz, J. Radebaugh, Dust devils in thin air: vortex observations at a high elevation Mars analog site in the Argentinian Puna. *Geophys. Res. Lett.* **43** (2016). doi:[10.1002/2015GL067412](https://doi.org/10.1002/2015GL067412)
- 2264 R.D. Lorenz, D. Reiss, Solar panel clearing events, dust devil tracks, and in-situ vortex detections on Mars. *Icarus* **248**, 162–164 (2015)
- 2265 R.D. Lorenz, K.S. Sotzen, Buoyant thermal plumes from planetary landers and rovers: application to sizing of meteorological masts. *Planet. Space Sci.* **90**, 81–89 (2014). doi:[10.1016/j.pss.2013.10.011](https://doi.org/10.1016/j.pss.2013.10.011)
- 2266 R.D. Lorenz, S. Kedar, N. Murdoch, P. Lognonné, T. Kawamura, D. Mimoun, W.B. Banerdt, Seismometer signature of dust devils: implication for InSight, in *2015 European and Planetary Science Conference*, Nantes (2015a)
- 2267 R.D. Lorenz, S. Kedar, N. Murdoch, P. Lognonné, T. Kawamura, D. Mimoun, W.B. Banerdt, Seismometer detection of dust devil vortices by ground tilt. *Bull. Seismol. Soc. Am. BSSA-S-15-00169* (2015b)
- 2268 R.D. Lorenz, L.D. Neakrase, J.D. Anderson, In-situ measurement of dust devil activity at La Jornada Experimental Range, New Mexico, USA. *Aeolian Res.* **19**, 183–194 (2015c)
- 2269 R.D. Lorenz, M. Balme, Z. Gu et al., History and application of dust devil studies. *Space Sci. Rev.* (2016). doi:[10.1007/s11214-016-0239-2](https://doi.org/10.1007/s11214-016-0239-2)
- 2270 J. Lowell, W.S. Truscott, Triboelectrification of identical insulators. II. Theory and further experiments. *J. Phys. D, Appl. Phys.* **19**, 1281–1298 (1986). doi:[10.1088/0022-3727/19/7/018](https://doi.org/10.1088/0022-3727/19/7/018)
- 2271 J.P. Mason, M.R. Patel, S.R. Lewis, Radiative transfer modelling of dust devils. *Icarus* **223**, 1–10 (2013)
- 2272 J.P. Mason, M.R. Patel, S.W. Lewis, The retrieval of optical properties from terrestrial dust devil vortices. *Icarus* **231**, 385–393 (2014)
- 2273 S. Maurice, R.C. Wiens, W. Rapin, D. Mimoun, X. Jacob, B. Betts, S. Clegg, A. Cousin, O. Gasnault, O. Forni, J. Lasue, P.-Y. Meslin, J.F. Bell, G. Delory, A microphone supporting LIBS investigation on Mars. *Lunar Planet. Sci. Conf.* **47**, 3044 (2016)
- 2274 J.P. Merrison, H.P. Gunnlaugsson, K. Kinch, T.L. Jacobsen, A.E. Jensen, P. Nørnberg, H. Wahlgreen, An integrated laser anemometer and dust accumulator for studying wind-induced dust transport on Mars. *Planet. Space Sci.* **54**(11), 1065–1072 (2006). doi:[10.1016/j.pss.2006.05.026](https://doi.org/10.1016/j.pss.2006.05.026)
- 2275 S.M. Metzger, Dust devils as aeolian transport mechanisms in southern Nevada and in the Mars Pathfinder landing site. Ph.D. thesis, Univ. of Nev., Reno (1999)
- 2276 S.M. Metzger, J.R. Carr, J.R. Johnson, T.J. Parker, M.T. Lemmon, Dust devil vortices seen by the Mars Pathfinder camera. *Geophys. Res. Lett.* **26**(18), 2781–2784 (1999)
- 2277 S.M. Metzger, M. Kurgansky, A. Montecinos, V. Villagram, H. Verdejo, Chasing dust devils in Chile’s Atacama Desert. LPSC Abstract 2564 (2010)
- 2278 S. Metzger, M. Balme, A. Pathare, N. Renno, M. Towner, A. Spiga, H. Elliott, High-resolution dust devil sampling for sediment loads, wind speeds, temperature and pressure excursions, in *42nd Lunar and Planetary Science Conference*. Texas (2011). Abstr. #1608
- 2279 G.J. Molina-Cuberos et al., A new approach for estimating Titan’s electrical conductivity based on data from relaxation probe sensors on the Huygens experiment. *Planet. Space Sci.* **58**(14–15) (2010). doi:[10.1016/j.pss.2010.09.014](https://doi.org/10.1016/j.pss.2010.09.014)
- 2280 J.E. Moores et al., Observational evidence of a suppressed planetary boundary layer in northern Gale Crater, Mars as seen by the Navcam instrument onboard the Mars Science Laboratory rover. *Icarus* **249**(15), 129–142 (2015). doi:[10.1016/j.icarus.2014.09.02](https://doi.org/10.1016/j.icarus.2014.09.02)

Field Measurements of Terrestrial and Martian Dust Devils

- 2301 J.R. Murphy, S. Nelli, Mars Pathfinder convective vortices: frequency of occurrence. *Geophys. Res. Letters* **29**(23) (2002). doi:[10.1029/2002GL015214](https://doi.org/10.1029/2002GL015214)
- 2302 J. Murphy, C.B. Leovy, J. Tillman, Observations of martian surface winds at the Viking Lander 1 site. *J. Geophys. Res.* **95**, B9 (1990). doi:[10.1029/JB095iB09o14555](https://doi.org/10.1029/JB095iB09o14555)
- 2303 L. Neakrase et al., Particle lifting processes in dust devils. *Space Sci. Rev.* (2016, accepted)
- 2304 L.D.V. Neakrase, R. Greeley, Dust devil sediment flux on Earth and Mars: laboratory simulations. *Icarus* **206**, 306–318 (2010). doi:[10.1016/j.icarus.2009.08.028](https://doi.org/10.1016/j.icarus.2009.08.028)
- 2305 A.M.C. Oke, D. Dunkerley, N.J. Tapper, Willy-willies in the Australian landscape: sediment transport characteristics. *J. Arid Environ.* **71**, 216–228 (2007)
- 2306 A.V. Pathare, M.R. Balme, S.M. Metzger, A. Spiga, M.C. Towner, N.O. Renno, F. Saca, Assessing the power law hypothesis for the size-frequency distribution of terrestrial and martian dust devils. *Icarus* **209**(2), 851–853 (2010)
- 2307 J.B. Pollack, D.S. Coburn, F.M. Flasar, R. Kahn, C.E. Carslton, D. Pidek, Properties and effects of dust particles suspended in the martian atmosphere. *J. Geophys. Res.* **84**(B6), 2929–2945 (1979)
- 2308 A. Powell, Theory of vortex sound. *J. Acoust. Soc. Am.* **36**(1), 177–195 (1964)
- 2309 J. Raack, D. Reiss, G.G. Ori, K. Taj-Eddine, Vertical grain size distributions in dust devils: analyses of in situ sampled from southern Morocco. EPSC Abstract, EPSC2012-427-1, 2014
- 2310 S. Rafkin, D. Banfield, J. Silver, K. Nowicki, R. Dissly, A. Stanton, in *An Instrument to Measure Turbulent Fluxes in the Atmosphere of Mars and Other Planets, European Planetary Science Congress 2013*. EPSC Abstracts, vol. 8, London, UK (2013), EPSC2013-575, Poster presentation, <http://meetingorganizer.copernicus.org/EPSC2013/EPSC2013-575.pdf>
- 2311 D. Reiss, A. Spiga, G. Erkeling, The horizontal motion of dust devils on Mars derived from CRISM and CTX/HiRISE observations. *Icarus* **277**, 8–20 (2014)
- 2312 N.O. Renno, M.L. Burkett, M.O. Larkin, A simple thermodynamical theory for dust devils. *J. Atmos. Sci.* **55**, 3244–3252 (1998)
- 2313 N.O. Renno, A.A. Nash, J. Lunine, J. Murphy, Martian and terrestrial dust devils: test of a scaling theory using Pathfinder data. *J. Geophys. Res.* **105**(E1), 1859–1865 (2000)
- 2314 N.O. Renno, V.J. Abreu, J. Koch, P.H. Smith, o.K. Hartogensis, H.A.R. De Bruin, D. Burose, G.T. Delory, W.M. Farrell, C.J. Watts, J. Garatuza, M. Parker, A. Carswell, MATADOR 2002: a pilot field experiment on convective plumes and dust devils. *J. Geophys. Res.* **109**, E07001 (2004). doi:[10.1029/2003JE002219](https://doi.org/10.1029/2003JE002219)
- 2315 T.J. Ringrose, M.C. Towner, J.C. Zarnecki, Convective vortices on Mars: a reanalysis of Viking Lander 2 meteorological data, sols 1–60. *Icarus* **163**(1), 78–87 (2003). doi:[10.1016/S0019-1035\(03\)00073-3](https://doi.org/10.1016/S0019-1035(03)00073-3)
- 2316 T.J. Ringrose, M. Patel, M. Towner, M. Balme, S. Metzger, J. Zarnecki, The meteorological signatures of dust devils on Mars. *Planet. Space Sci.* **55**, 14 (2007)
- 2317 J.A. Rodriguez-Manfredi et al., MEDA: an environmental and meteorological package for Mars 2020, in *45th Lunar and Planetary Science Conference*, The Woodlands, Texas, USA (2014). Poster presentation, <http://ssed.gsfc.nasa.gov/IPM/PDF/1125.pdf>
- 2318 J.A. Ryan, J.J. Carroll, Dust devil wind velocities: mature state. *J. Geophys. Res.* **75**, 531–541 (1970)
- 2319 J.A. Ryan, R.D. Lucic, Possible dust devils, vortices on Mars. *J. Geophys. Res.* **88**(C15), 11005–11011 (1983)
- 2320 D.S. Schmidt, R.A. Schmidt, J.D. Dent, Electrostatic force on saltating sand. *J. Geophys. Res.* **103**(D8), 8997–9001 (1998)
- 2321 J.T. Schofield, J.R. Barnes, D. Crisp, R.M. Haberle, S. Larsen, J.A. Magalhaes, J.R. Murphy, A. Seiff, G. Wilson, The Mars Pathfinder atmospheric structure investigation meteorology (ASI/MET) experiment. *Science* **278**(5344), 1752–1758 (1997). doi:[10.1126/science.278.5344.1752](https://doi.org/10.1126/science.278.5344.1752)
- 2322 R.L. Schwiesow, R.E. Cupp, M.J. Post, P.C. Sinclair, R.F. Abbey, Velocity structures of waterspouts and dust devils as revealed by Doppler lidar measurements. *Bull. Am. Meteorol. Soc.* **58**, 677 (1977)
- 2323 A. Seiff, J.E. Tillman, J.R. Murphy, J.T. Schofield, D. Crisp, J.R. Barnes, C. LaBaw, C. Mahoney, J.D. Mihalov, G.R. Wilson, R. Haberle, The atmosphere structure and meteorology instrument on the Mars Pathfinder lander. *J. Geophys. Res.* **103**(E2), 4045–4056 (1997)
- 2324 Y.P. Shao, *Physics and Modelling of Wind Erosion*, 2nd edn. (Springer, Heidelberg, 2008)
- 2325 Y. Shao, M.R. Raupach, P.A. Findlater, Effect of saltation bombardment on the entrainment of dust by wind. *J. Geophys. Res.* **98**, 12719–12726 (1993)
- 2326 P.C. Sinclair, On the rotation of dust devils. *Bull. Am. Meteorol. Soc.* **46**, 388–391 (1965)
- 2327 P.C. Sinclair, A quantitative analysis of the dust devil. Ph.D. Dissertation, University of Arizona, 1966, p. 292
- 2328 P. Sinclair, General characteristics of dust devils. *J. Appl. Meteorol.* **8**, 32–45 (1969)
- 2329 P. Sinclair, The lower structure of dust devils. *J. Atmos. Sci.* **30**, 1599–1619 (1973)
- 2330 P.H. Smith et al., Introduction to special section on the Phoenix Mission: landing site characterization experiments, mission overviews, and expected science. *J. Geophys. Res.* **113**(E3) (2008)

- 2351 P.H. Smith, M.T. Lemmon, Opacity of the Mars atmosphere measured by the imager for Mars Pathfinder.  
2352 J. Geophys. Res. **104**, 8975–8985 (1999)
- 2353 P.H. Smith, M.G. Tomasko, D. Britt, D.G. Crowe, R. Reid, H.U. Keller, N. Thomas, F. Gliem, P. Rueffer,  
2354 R. Sullivan, R. Greeley, J.M. Knudsen, M.B. Madsen, H.P. Gunnlaugsson, S.F. Hviid, W. Goetz, L.A.  
2355 Soderblom, L. Gaddis, R. Kirk, The imager for Mars Pathfinder experiment. J. Geophys. Res. **102**(E2),  
2356 4003–4025 (1997)
- 2357 M.D. Smith, M.J. Wolff, M.T. Lemmon, N. Spanovich, D. Banfield, C.J. Budney, R.T. Clancy, A. Ghosh,  
2358 G.A. Landis, P. Smith, B. Whitney, P.R. Christensen, S.W. Squyres, First atmospheric sciences re-  
2359 sults from the Mars Exploration Rovers mini-TES. Science **306**(5702), 1750–1753 (2004). doi:[10.1126/  
2360 science.1104527](https://doi.org/10.1126/science.1104527)
- 2361 P.H. Smith, L.K. Tamppari, R.E. Arvidson, D. Bass, D. Blaney, W.V. Boynton, A. Carswell, D.C. Catling,  
2362 B.C. Clark, T. Duck, E. DeJong, D. Fisher, W. Goetz, H.P. Gunnlaugsson, M.H. Hecht, V. Hipkin, J.  
2363 Hoffman, S.F. Hviid, H.U. Keller, S.P. Kounaves, C.F. Lange, M.T. Lemmon, M.B. Madsen, M. Malin,  
2364 W.J. Markiewicz, J. Marshall, C.P. McKay, M.T. Mellon, D.W. Ming, R.V. Morris, N. Renno, W.T. Pike,  
2365 U. Staufer, C. Stoker, P. Taylor, J. Whiteway, A.P. Zent, Water at the Phoenix landing site. Science **325**,  
2366 58–61 (2009)
- 2367 J.T. Snow, T.M. McClelland, Dust devils at white sands missile range, New Mexico: 1. Temporal and spatial  
2368 distributions. J. Geophys. Res. **95**, 13,707–13,721 (1990)
- 2369 G.G. Sorrells, A preliminary investigation into the relationship between long-period noise and local fluctua-  
2370 tions in the atmospheric pressure field. Geophys. J. **26**, 71–82 (1971)
- 2371 G.G. Sorrells, J.A. McDonald, Z.A. Der, E. Herrin, Earth motion caused by local atmospheric pressure  
2372 changes. Geophys. J. **26**, 83–98 (1971)
- 2373 S.W. Squyres et al., The Spirit rover’s Athena science investigation at Gusev Crater, Mars. Science **305**,  
2374 794–799 (2004)
- 2375 K. Steakley, J. Murphy, A year of convective vortex activity at Gale Crater. Icarus **278**, 180–193 (2016)
- 2376 R. Sullivan, R. Greeley, M. Kraft, G. Wilson, M. Golombek, K. Herkenhoff, J. Murphy, P. Smith, Results of  
2377 the imager for Mars Pathfinder windsock experiment. J. Geophys. Res. **105**(E10), 24547–24562 (2000).  
2378 doi:[10.1029/1999JE001234](https://doi.org/10.1029/1999JE001234)
- 2379 P.A. Taylor, D.C. Catling, M. Daly, C.S. Dickinson, H.P. Gunnlaugsson, A.M. Harri, C.F. Lange, Temperature,  
2380 pressure, and wind instrumentation in the Phoenix meteorological package. J. Geophys. Res. **113**,  
2381 E00A10 (2008). doi:[10.1029/2007JE003015](https://doi.org/10.1029/2007JE003015)
- 2382 P.A. Taylor et al., On pressure measurement and seasonal pressure variations during the Phoenix mission.  
2383 J. Geophys. Res. **115**, E00E15 (2010). doi:[10.1029/2009JE003422](https://doi.org/10.1029/2009JE003422)
- 2384 J.E. Tillman, N.C. Johnson, P. Guttorp, D.B. Percival, The martian annual atmospheric pressure cycle: years  
2385 without great dust storms. J. Geophys. Res. **98**(E6), 10963–10971 (1993). doi:[10.1029/93JE01084](https://doi.org/10.1029/93JE01084)
- 2386 A.D. Toigo, M.I. Richardson, S.P. Ewals, P.J. Gierasch, Numerical simulation of martian dust devils. J. Geo-  
2387 phys. Res., Planets **108**(E6) (2003)
- 2388 M.C. Towner, Characteristics of large martian dust devils using Mars odyssey thermal emission imaging  
2389 system visual and infrared images. J. Geophys. Res. **114**, E02010 (2008)
- 2390 D.M. Tratt, M.H. Hecht, D. Catling, E.C. Samulon, P.H. Smith, In situ measurement of dust devil dynamics:  
2391 toward a strategy for Mars. J. Geophys. Res. **108**(E11), 5116 (2003)
- 2392 D.T. Tyler, J.R. Barnes, Mesoscale modeling of the circulation in the Gale Crater region: an investigation  
2393 into the complex forcing of convective boundary layer depths. Mars **8**, 58–77 (2013). doi:[10.1555/mars.  
2394 2013.0003](https://doi.org/10.1555/mars.2013.0003)
- 2395 D.T. Tyler, J.R. Barnes, Convergent crater circulations on Mars: influence on the surface pressure cycle and  
2396 the depth of the convective boundary layer. Geophys. Res. Lett. **42**, 7343–7350 (2015)
- 2397 J. Whiteway, M. Daly, A. Carswell, T. Duck, C. Dickinson, L. Konguem, C. Cook, Lidar on the Phoenix  
2398 mission to Mars. J. Geophys. Res. **113**, E00A08 (2008). doi:[10.1029/2007JE003002](https://doi.org/10.1029/2007JE003002)
- 2399 N.R. Williams, Development of dust whirls and similar small-scale vortices. Bull. Am. Meteorol. Soc. **29**,  
2400 106–117 (1948)
- 2401 J.P. Williams, Acoustic environment of the martian atmosphere. J. Geophys. Res. **106**(E3), 5033–5041 (2001)
- 2402 C.L. Wilson, A. Davis, D. Hutchins, M.C. Towner, An ultrasonic anemometer for Mars. J. Acoust. Soc. Am.  
2403 **123**(5), 3401 (2008). doi:[10.1121/1.2934100](https://doi.org/10.1121/1.2934100)
- 2404 R.E. Wyatt, Pressure drop in a dust devil. Mon. Weather Rev., 7–8 January 1954
- 2405 L.M. Zelenyi, O.I. Korabiev, D.S. Rodionov, B.S. Novikov, K.I. Marchenkov, O.N. Andreev, E.V. Larionov,  
2406 Scientific objectives of the scientific equipment of the landing platform of the ExoMars-2018 mission.  
2407 Sol. Syst. Res. **49**(7), 509–517 (2015)
- 2408 M-P. Zorzano, F.J. Martín-Torres, H. Kahanpää, J. Moores, S. Navarro, A. Lepinette, E. Sebastian, J. Gómez-  
2409 Elvira, REMS Team, The MSL Science Team), Radiation obscuration by dust devils at Gale as observed  
2410 by the REMS UV sensor, in *EGU General Assembly 2013*. Geophysical Research Abstracts, vol. 15  
2411 (2013), EGU2013-11155, <http://meetingorganizer.copernicus.org/EGU2013/EGU2013-11155.pdf>